The International Congress for global Science and Technology

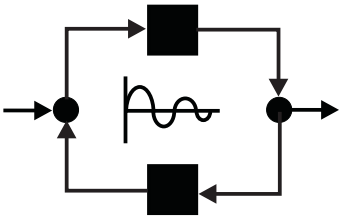

ICGST International Journal on Automatic Control & System Engineering (ACSE)

Volume (8), Issue (I)
July, 2008

wwww.icgst.com
www.icgst-amc.com
www.icgst-ees.com

ACSE Journal
ISSN: Print 1687-4811
ISSN Online 1687-482X
ISSN CD-ROM 1687-4838

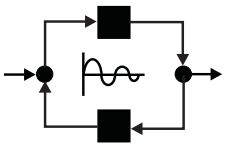

Table of Contents

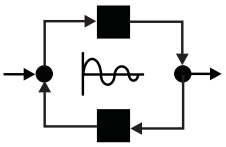

ICGST International Journal on Automatic Control & System Engineering - (ACSE)

A publication of the International Congress for global Science and Technology - (ICGST)

ICGST Editor in Chief: Dr. Ashraf Aboshosha

www.icgst.com. editor@icgst.com

Guest Editor: Prof. Dr. Z. Gao,

School of Electrical Engineering & Automation of Tianjin University, China

www.icgst.com

Employing a ROM-based Frequency Meter for Precise Tracking of Line Frequency

Mahmoud Abaza

Athabasca University, #1 University Drive, Athabasca, Canada
mahmouda@athabascau.ca,
http://www.athabascau.ca

Abstract
In this paper, a new simple method for accurate measurement of line frequencies is proposed. The method is based on storing the line frequencies to be measured in read-only memory ROM. For comparison, three alternative measurement methods are illustrated

Keywords: *Power line frequency, Read Only Memory, Power Control, Embedded Systems.*

1. Introduction
There are different methods to measure line frequency of power systems. The most versatile of those are built around microprocessors. Microprocessors allow to add many functions beside measuring frequencies, such as adding an alarm, history and so on. Some of specialized frequency measurement appeared in the literature such as measurement under non stationary situations [6], and frequency mixing and sub-sampling [7]. Most of the time, however, it suffices to know the line frequency instantly and accurately. Our approach provides smart, cheap, fast and accurate method to measure the line frequency. As early ROM-based solutions allowed only small deviation from nominal frequency, recent advances in storage technology provides a huge accurate readings. Our approach provides instant measurement, because all what it takes is the propagation delay within the ROM. This, in particular, is important under instability conditions. We will present theoretical bases for the work, followed by a complete design and analysis of the circuit. At the end we will have conclusion and future research.

The rest of the paper is organised as follows; Section 2 presents the theoretical analysis of the subject which includes discussion about processor-based solution, the simplified frequency meter, ROM-based frequency meter basics and implementation. Section 3 formulates the conclusion.

2. Theory
The operation of the proposed frequency meter is based on measuring the time period, *T*, of the line frequency to be found. The time period can be simply measured by counting the number of pulses *N* of a given clock frequency f_c in one time period. Therefore, the time period is given by

$$T = \frac{N}{f_c} \tag{1}$$

It is obvious from this equation that the resolution in the period measurement is $\frac{1}{f_c}$ seconds. We will try in the following to device effective methods to carry the division operation of formula one in an effective and economic way.

2.1. Processor-based Solution
The processor-based frequency measurement is straightforward. Figure 3, presents a block diagram of a typical solution. The CPU counts number of pulses during one signal period. All operations including division and multiplication can be easily programmed, and the result in the desired format is produced by the CPU IO. Suitable and economic CPUs for this purpose do not have built-in division operations. Therefore, division is done through a sequence of shift and subtract operations, taking significant number of CPU cycles.

The CPU solution is versatile and it is easy to implement. The CPU can also be doing other useful work, such as issuing warning for certain frequency values, producing statistics of line frequency status, recording history of line frequency vibrations and others.

2.2. A simplified frequency meter

In an earlier work, a simplified frequency meter has been devised .The division operation of Formula 1, has been approximated by a single addition operation.

In Figure 4, The up/down counter with parallel load finds the difference, *d* , between the expected number clock pulses of the optimal frequency and the actual pulse count during one signal period. Hence,

$$f = \frac{1}{T_0 \pm \frac{d}{fc}} \tag{2}$$

Using Taylor series expansion, and approximating by taking only the first two terms, the measured frequency becomes:

$$f \approx \frac{1}{T_0} \mp \frac{d}{T_0^2 f_c} \approx f_0 \mp \alpha.d \tag{3}$$

It is not difficult to scale *d* by a certain constant. Finally, finding f is turned into and add or subtract operation which can be done by a simple add/subtract circuit.

2.3. ROM-based frequency meter

For the measurement of a line frequency with known nominal value of f_0 Hz and frequency deviation of $\pm D$ Hz, it is only needed to store a mapping table for the frequency range which extends from $f_0 - D$ to $f_0 + D$ Hz. The number of line frequencies *M* needed to be stored in the ROM is determined by the range of frequencies to be measured *2D* and the resolution in the period of measurement:

$$M = \frac{2Df_c}{f_0^2 - D^2} + 1 \tag{4}$$

The value of the line frequencies f_i to be stored in the M locations of the ROM are given by

$$f_i = \frac{f_c(f_0 + D)}{f_c + i(f_0 + D)} \tag{5}$$

With i = 0, 1, 2, 3, …, *M-1*

The maximum line frequency $f_0 + D$ Hz is stored in the first memory location having address 0 and the minimum line frequency $f_0 - D$ Hz is stored in the last t memory location having the address *M-1*.

By choosing the ROM size *M* to the power of 2 ($M = 2^n$), the number of address lines will be *n.* The wordlength of each memory location is determined by the number of decimal digits representing the line frequency to be stored. For the simplicity of design, BCD format will be used to represent decimal digits. To store line frequency of *m* decimal digits, memory locations of *4m* bits wordlength will be needed.

Let us summarise the above discussion by designing a frequency meter for the line frequency of $f_0 = 60$ Hz with $D = \pm 5$ Hz deviation. Let us assume that 1024 line frequencies in the range from 55 to 65 Hz are to be stored in ROM. This requires a ROM with 1024 locations and wordlength of *4m* bits. The number of address lines of ROM is 10, that is, $(\log_2 1024)$ From equation 2, the clock frequency is found to be 365722 Hz. This clock frequency gives a resolution in the time period measurement of $\frac{1}{365722}$ seconds. It is obvious from equation 3 that the resolution in the frequency measurement is not fixed and it has a worst-case resolution of 0.012 Hz. At 60 Hz. Therefore, in this case, four decimal digits are adequate to represent the line frequency.

2.4. Implementation of ROM-based meter

The purpose of line frequency meter can be easily implemented as shown in Fig 1. The main blocks in Figre 1 are 1) two one-shot multivibrators 2)*n*-stage binary counter 3)ROM with *n*-address lines and *4m*-bit wordlength 4) *m*- 4-bit binary latches and 5) *m* seven-segment drivers and displays. The input signal whose frequency to be measured is applied to the conditioning circuit to produce TTL compatible signal. The TTL compatible signal is applied to a one-shot multivibrator (OS1) to generate pulses with very short duration (less than the time period of the clock frequency) with the same frequency as the input signal. The signal will be used to latch the output of the ROM. The output of OS1 is applied to a second shot (OS2) to generate pulses with duration equals to $\frac{1}{f_0 + D}$. This signal is used to clear and disable the counter as long as pulse is high. A stable high-frequency crystal clock whose frequency is determined from equation 2 given f_0 , M and D, is applied to the count-enable input of the counter. The timing diagram for the operation of the proposed frequency meter is shown in Fig 2. The counter counts only when the output of the OS2 is low and it is cleared and disabled when it is high. The number of counts in this time period represents the address of the line frequency which is stored in one of the *M* locations of the ROM. The line frequencies are stored in the ROM BCD format. The latched frequency is applied to the BCD-to-seven segment drivers followed by seven segment displays. The line frequencies is to be stored in ROM are shown in Table 1. It is obvious from the table that four decimal digits are needed to represent the line frequencies with an acceptable accuracy.

3. Conclusion

An accurate, low cost frequency meter for the measurement of line frequency is proposed. A ROM is used to store a range of line frequencies around the nominal line frequency. The number of line frequencies is determined by the acceptable deviation of the line frequency from the nominal value and the required

resolution. The proposed meter can be easily modified to measure other frequencies with known nominal values by changing ROM contents and clock frequency. Other bad conditions in line frequency, such as resisting harmonics or low/high inductance, or distortion will be left for future research.

4. References

[1] T. Kaspairs, N. C Voulgaris and C. C. Hamilakis. " A method of precise measurement of the differences between two low frequencies", IEEE Trans. On Instrumentation and Measurement, Vol. IM-34, No. 1, March 1958

[2] V.K.Govindan, N. V. Vaidan and Velyaudhan,". A novel method for digital monitoring frequency deviation in power systems", Internationl Journal of Electronics, Vol. 56. 1, pp 127-134,1984.

[3] M. Irshid, W. A. Shahab and B. R. El-Asir, " A simple programmable frequency meter for low frequencies with known nominal values", IEEE Trans, on Instrumentation, Vol IM-40, No. 3, pp 640-642, June 1991.

[4] Mansour I., "An Accurate Method for Measurement of Line Frequency using Read-Only Memory", POWER AND ENERGY SYSTEMS ~ PES 2007 ~January3-5,2007,Clearwater, Florida.

[5] "Instantaneous line-frequency measurement under nonstationary situations", Lopez, A. Montano, J.C. Castilla, M. Gutierrez, J. Borras, D. Bravo, J.C. , Dpto. Tecnologia Electronica, Escuela Universitaria Politecnica, Sevilla, Spain; " Instrumentation and Measurement Technology Conference, 2004. IMTC 04. Proceedings of the 21st IEEE, Publication Date: 18-20 May 2004, Volume: 2, On page(s): 941- 944 Vol.2, ISSN: 1091-5281, ISBN: 0-7803-8248-X

[6] Frequency Mixing and Sub-Sampling Based RF-Measurement APPARATUS FOR IEEE 1149.4, Juha Hakkinen1, Pekka Syri1, Juha-Veikko Voutilainen2 and Markku Moilanen, Department of Electrical and Information Engineering, Electronics Laboratory1, Optoelectronics and Measurement Techniques Laboratory, University of Oulu, Finland

Table 1. Example ROM contents

Address	Line Frequency
0	56.000
1	64.988
2	64.977
3	64.965
.	.
.	.
467	60.018
468	60.009
469	59.999
470	59.989
.	.
.	.
1020	55.025
1021	55.017
1022	55.008
1023	55.000

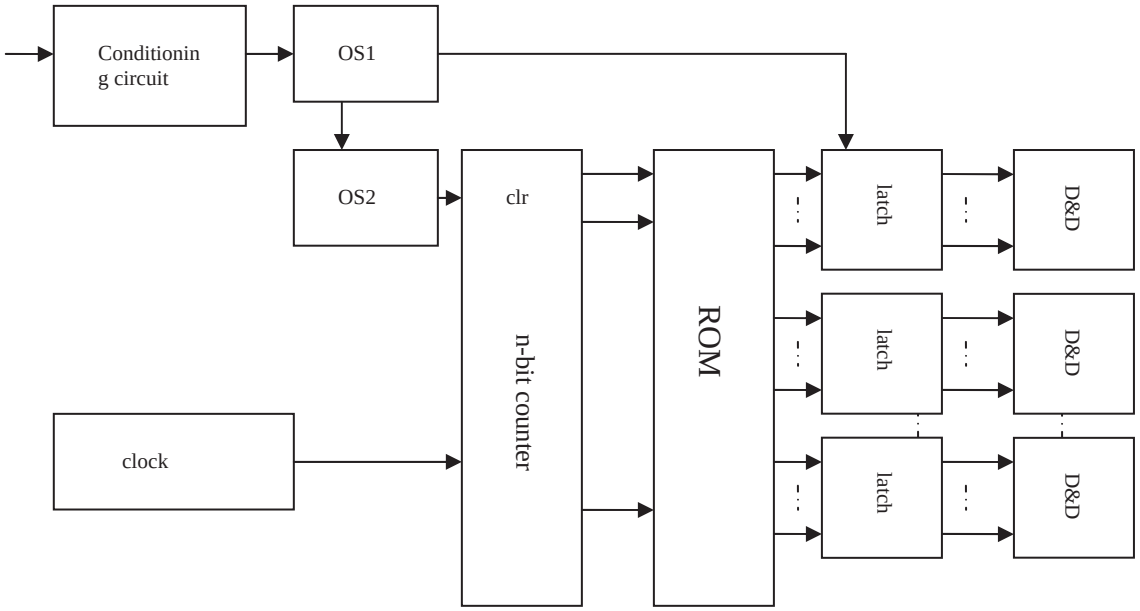

Figure 1. ROM-based line frequency meter

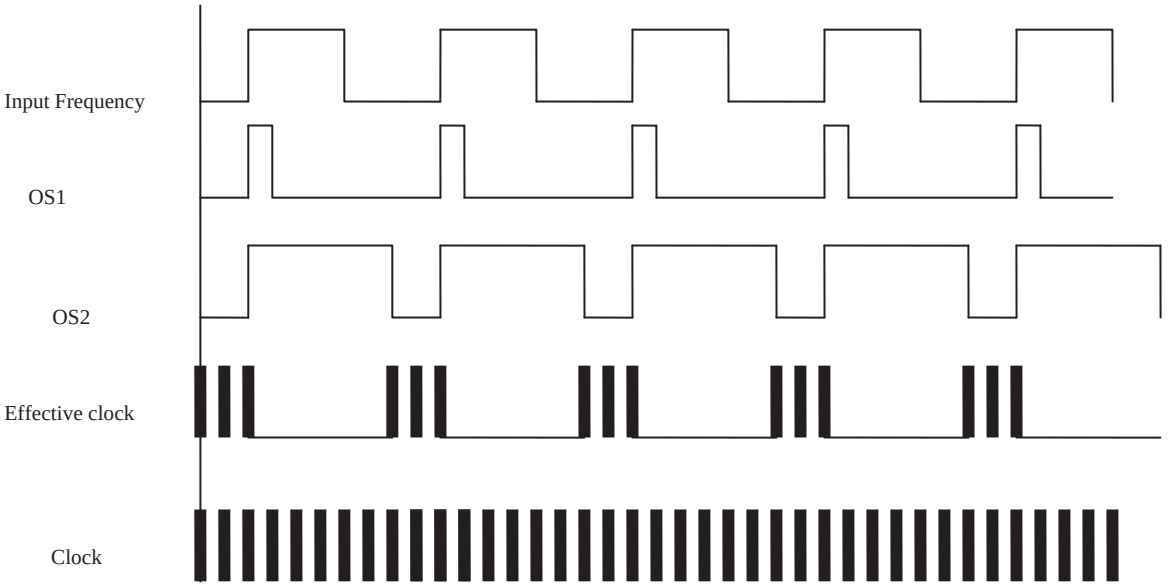

Figure 2. Timing diagram for the frequency meter.

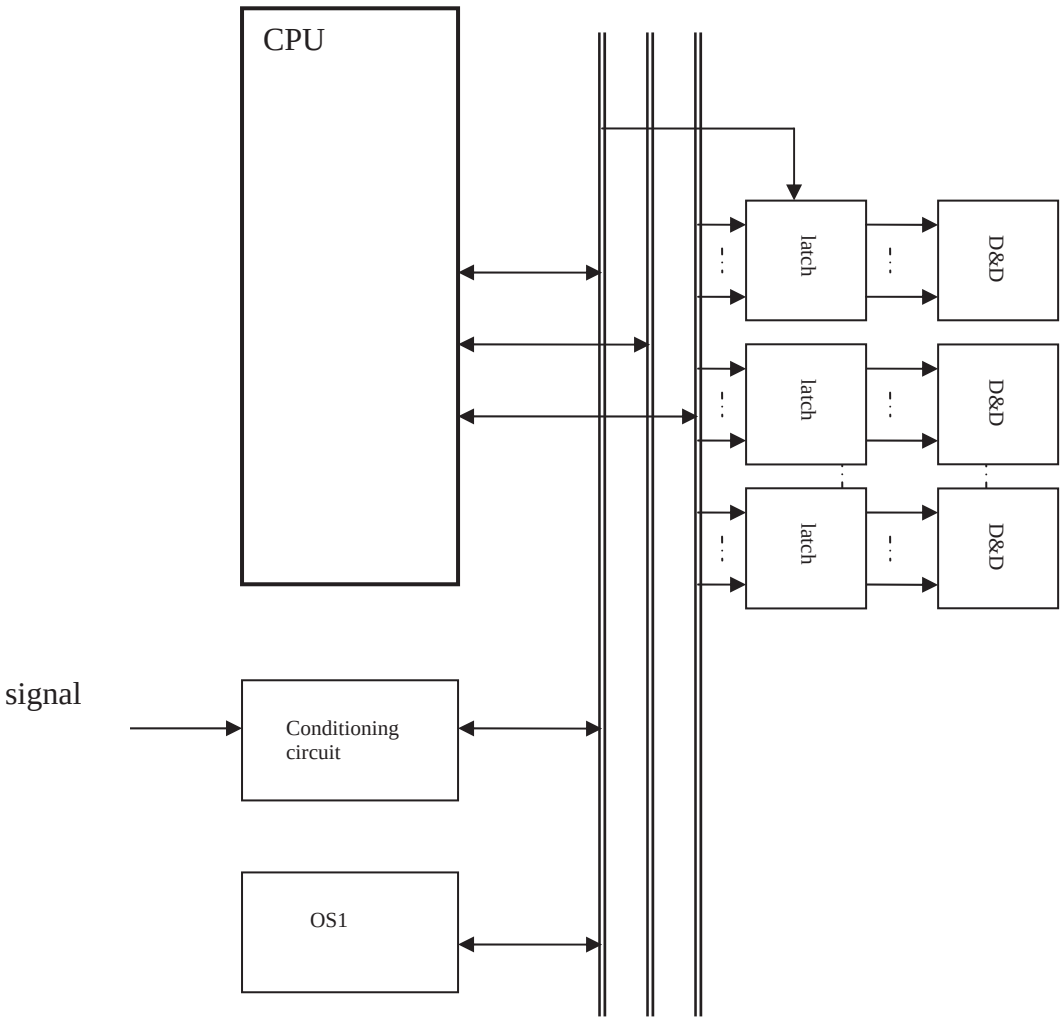

Figure 3. CPU-based line frequency meter.

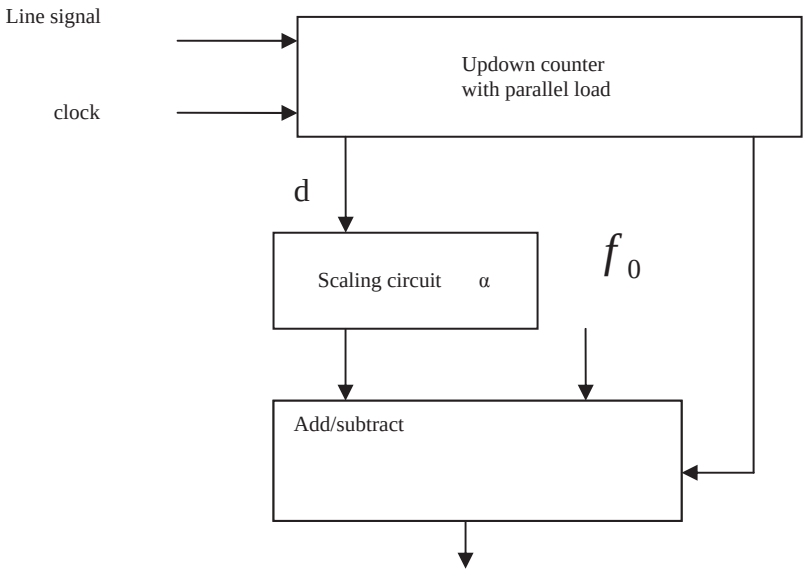

Figure 4. Simplified Frequency meter block diagram

www.icgst.com

Capacitor Placement in Balanced and Unbalanced Radial Distribution System by Discrete Particle Swarm Optimization

A. Dr. S.Sivanagaraju [1], B. J.Viswanatha Rao[2] *
A.Associate Professor, Department of EEE, J.N.T.U. College of Engineering, Anantapur-515001, A.P., India.
B.Associate Professor, Department of EEE, Swarnandhra College of Engineering & Technology,Narsapur-534280,India.
*corresponding author: viswanath_72@yahoo.com

Abstract
Capacitor placement problem is a non-linear and non-differentiable mixed integer optimization problem with a set of equality and inequality constraints. Most conventional optimization techniques are incapable to solve this hard combinatorial problem. The radial distribution systems are unbalanced because of single-phase, two-phase and three-phase loads. Thus, load flow solution for balance radial distribution networks will not be sufficient to solve the unbalanced case and, hence, special treatment is required for solving such networks. Optimal capacitor placement can result in system loss reduction, power factor correction, voltage profile improvement, and feeder capacity release. In this paper, Particle Swarm Optimization (PSO) based approach is used to achieve optimal capacitor placement for balanced and unbalanced radial distribution systems. The size of capacitors can be determined by using particle swarm optimization algorithm. In this fitness function is to maximize the net savings. In order to obtain the fitness values, load flow calculations has to be carried and capacitor placement is almost certain that better loss reduction can be obtained. The proposed solution method employs to search for optimal locations, types, and sizes of capacitors to be placed and optimal numbers of switched capacitor banks at different load levels. The proposed approach has been implemented and tested on various test systems with promising results.

***Keywords**: Capacitor placement, load flows, radial distribution system, Discrete Particle swarm optimization (DPSO)*

1. Introduction

Due to high concentration of inductive loads in distribution system, energy losses are more. Shunt capacitors are widely used in distribution system consuming negative VAR, which counteracts some of the lagging components of inductive VAR at the point of installation. Thus, it modifies the characteristics of inductive load. Shunt capacitor results in to a number of benefits like improvement of power factor, reduction of power loss, improvement of voltage profile, improvement of voltage stability and system-released capacity. To achieve these benefits to the utmost extent under various operating constraints, distribution engineers are required to determine the optimal locations, types and sizes of capacitors to be placed and control settings of switched capacitors at different load levels.

In the past lot of work has been carried in the area of reactive power compensation for radial distribution networks [1-3]. These methods are based on different non-linear programming techniques and provide only a local optimum solution with a less computation burden. Recently, researchers have attempted to obtain optimum values of shunt capacitors for radial distribution networks using Simulated Annealing and Genetic Algorithms (GA).Chiang have used the method of simulated annealing to obtain the optimum values of shunt capacitors for radial distribution networks. SundhaRajan and Pahwa [4] have used Genetic Algorithm for obtaining optimum value of capacitors. They [4] treated capacitors as constant reactive power load and no method is suggested to reduce CPU time. GA is capable of determining a near global solution with lesser computational burden than the simulated annealing method [4]. Capacitor placement problem is a non-linear and –differentiable mixed integer optimization problem with a set of equality and inequality constraints. Most conventional optimization techniques are incapable to solve this hard combinatorial problem. But particle swarm optimization (PSO) algorithm proposed by Eberhart and Kennedy is very suitable [5, 6]. The radial distribution systems are unbalanced because of single-phase, two-phase and three-phase loads. Thus, load flow solution for balance radial distribution networks will not be sufficient to solve the unbalanced case and, hence, special treatment is required for solving such networks. D.Thukaram, H.M.Wijekoon Banda and Jovitha Jerome proposed a robust three phase power flow algorithm for radial distribution systems [8]. Optimal capacitor placement

can result in system loss reduction, power factor correction, voltage profile improvement, and feeder capacity release. Xin-me Yu, Xin-yin Xiong, Yao-wu Wu proposed a PSO-based approach to optimal capacitor placement with harmonic distortion consideration [8].

In this paper, a modern AI-based method, particle swarm optimization is used to solve the capacitor placement with all the realistic problem formulation considerations. The size of capacitors can be determined by using particle swarm optimization algorithm for balanced and unbalanced radial distribution system. In this fitness function is to maximize the net savings. In order to obtain the fitness values, load flow calculations has to be carried and capacitor placement is almost certain that better loss reduction can be obtained.

The paper is organized as follows: Section (2) focuses on load flow method for balanced and unbalanced radial distribution system. Section (3 & 4) describes on development and performance of discrete particle swarm optimization (DPSO). Section (5) gives the applying DPSO for the capacitor placement problem. Section (6) gives the results and analysis & section (7) listing of the references used in the paper.

2. Load Flow Method

In this section load flow technique for balanced and unbalanced radial distribution systems are discussed.

2.1. Balanced Radial Distribution System

In any radial distribution system, the electrical equivalent of a branch-1, which is connected between node 1 and 2 having a resistance $r_{(1)}$ and inductive reactance $x_{(1)}$ is shown in Figure.1.From Figure.1 current flowing branch-1is given by

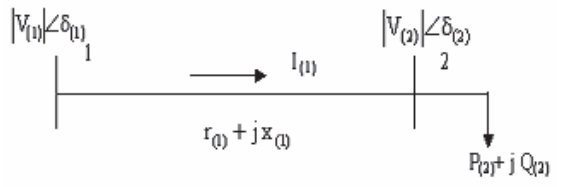

Figure 1. Single line diagram of branch-1

$$I_{(1)} = |V_{(1)}|\angle\delta_{(1)} - |V_{(2)}|\angle\delta_{(2)} / (r_{(1)} + jx_{(\ )}) \quad (1)$$

$$I_{(1)} = (P_{(2)} - jQ_{(2)}) / V_{(2)} * \angle\delta_{(2)} \quad (2)$$

From Equations. (1) and (2)

$$\frac{P_{(2)} - jQ_{(2)}}{|V_{(2)}|\angle -\delta_{(2)}} = \frac{|V_{(1)}|\angle -\delta_{(1)} - |V_{(2)}|\angle -\delta_{(2)}}{r_{(1)} + jx_{(1)}}$$

Separating real and imaginary parts, the real part is

$$|V_{(1)}||V_{(2)}|\cos(\delta_{(1)} - \delta_{(2)}) = |V_{(2)}|^2 + \{P_{(2)}r_{(1)} + Q_{(2)}x_{(1)}\} \quad (3)$$

and the imaginary part is

$$|V_{(1)}||V_{(2)}|\sin(\delta_{(1)} - \delta_{(2)}) = \{P_{(2)}x_{(1)} - Q_{(2)}r_{(1)}\} \quad (4)$$

$$\Rightarrow |V(2)|^4 + 2|V(2)|^2 (r(1)P(2) + x(1)Q(2) - 0.5|V(1)|^2) + (r(1)^2 + x(1)^2)(P(2)^2 + Q(2)^2) = 0 \quad (5)$$

Equation (5) has a straightforward solution and does not depend on the phase angle, which simplifies the problem formulation. In a distribution system, the voltage angle is not so important because the variation of voltage angle from the substation to the tail end of the distribution feeder is only few degrees. Note that from the two solution of $|V_{(2)}|^2$ only the one considering the sign of the square root of the solution of the quadratic equation gives a realistic value. The same is applicable when solving for $|V_{(2)}|$. Therefore from Equation (5), the solution of $|V_{(2)}|$ can be written as

$$|V_{(2)}| = \{\{(r_{(1)}P_{(2)} + x_{(1)}Q_{(2)} - 0.5|V_{(1)}|^2)^2 - (r_{(1)}^2 + x_{(1)}^2)(P_{(2)}^2 + Q_{(2)}^2)\}^{1/2} - (r_{(1)}P_{(2)} + x_{(1)}Q_{(2)} - 0.5|V_{(1)}|^2)\}^{1/2} \quad (6)$$

In general

$$|V_{(i+1)}| = \{\{(r_{(j)}P_{(i+1)} + x_{(j)}Q_{(i+1)} - 0.5|V_{(i)}|^2)^2 - (r_{(j)}^2 + x_{(j)}^2)(P_{(i+1)}^2 + Q_{(i+1)}^2)\}^{1/2} - (r_{(j)}P_{(i+1)} + x_{(j)}Q_{(i+1)} - 0.5|V_{(i)}|^2)\} \quad (7)$$

where, node no., i=1,2,…,nd
branch no., j=1,2…,nd-1
nd= total no. of nodes

The active and reactive power losses in branch 'j' are given by

$$\text{Ploss}[j] = \frac{r_{(j)}\{P^2_{(i+1)} + Q^2_{(i+1)}\}}{|V_{(i+1)}|^2} \quad (8)$$

$$\text{Qloss}[j] = \frac{x_{(j)}\{P^2_{(i+1)} + Q^2_{(i+1)}\}}{|V_{(i+1)}|^2} \quad (9)$$

The total active and reactive power losses of the system are :

$$\text{TPL} = \sum_{j=1}^{nd-1} Ploss[j] \quad (10)$$

$$\text{TQL}=\sum_{j=1}^{nd-1} Qloss[j] \tag{11}$$

Where Ploss[j], Qloss[j] =Active and reactive power losses of branch 'j'
TPL, TQL = Total active and reactive power losses of the system

2.2. Un-Balanced Radial Distribution System

In many cases, it is observed that the radial distribution systems are unbalanced because of single-phase, two-phase and three-phase loads. Thus, load flow solution for balance radial distribution networks will not be sufficient to solve the unbalanced case and, hence, special treatment is required for solving such networks. To solve the recursive algebraic equations the following information is necessary:

- Status of the feeder line, overloading of the conductor and feeder line currents.
- Whether the system can maintain adequate voltage level for the remote loads.
- The line losses in each segment.

Circuit model is shown in Figure 2 for a three-phase, four-wire grounded star system. Line charges are neglected at the distribution voltage level. For this four-wire system, Carson's equations lead to the development of an impedance matrix of 4×4 dimension. This matrix is used to calculate conductor voltage drop as shown below. By using Krichhoff's voltage law,

$$\begin{bmatrix} V_i^{ag} - V_j^{ag} \\ V_i^{bg} - V_j^{bg} \\ V_i^{cg} - V_j^{cg} \\ V_i^{ng} - V_j^{ng} \end{bmatrix} = \begin{bmatrix} ze_{ij}^{aa} & ze_{ij}^{ab} & ze_{ij}^{ac} & ze_{ij}^{an} \\ ze_{ij}^{ba} & ze_{ij}^{bb} & ze_{ij}^{bc} & ze_{ij}^{bn} \\ ze_{ij}^{ca} & ze_{ij}^{cb} & ze_{ij}^{cc} & ze_{ij}^{cn} \\ ze_{ij}^{na} & ze_{ij}^{nb} & ze_{ij}^{nc} & ze_{ij}^{nn} \end{bmatrix} \begin{bmatrix} I_{ij}^{a} \\ I_{ij}^{b} \\ I_{ij}^{c} \\ I_{ij}^{n} \end{bmatrix} \tag{12}$$

In a grounded neutral system, the voltages at neutral and ground are same,

$$V_i^{ng} - V_j^{ng} = 0 \tag{13}$$

by substituting Equation (13) in (12)

$$\begin{bmatrix} V_i^{ag} - V_j^{ag} \\ V_i^{bg} - V_j^{bg} \\ V_i^{cg} - V_j^{cg} \end{bmatrix} = \begin{bmatrix} V_{ij}^{a} \\ V_{ij}^{b} \\ V_{ij}^{c} \end{bmatrix} = \begin{bmatrix} ze_{ij}^{aa} & ze_{ij}^{ab} & ze_{ij}^{ac} & ze_{ij}^{an} \\ ze_{ij}^{ba} & ze_{ij}^{bb} & ze_{ij}^{bc} & ze_{ij}^{bn} \\ ze_{ij}^{ca} & ze_{ij}^{cb} & ze_{ij}^{cc} & ze_{ij}^{cn} \end{bmatrix} \begin{bmatrix} I_{ij}^{a} \\ I_{ij}^{b} \\ I_{ij}^{c} \end{bmatrix} \tag{14}$$

Where the values of the impedance elements are computed using the following expression based upon Carson's equation.

$$z_{ij}^{aa} = ze_{ij}^{aa} - \frac{ze_{ij}^{an} \times ze_{ij}^{na}}{ze_{ij}^{nn}} \tag{15}$$

Real and reactive power losses for phases a , b and c can be written as:

$$SL_{ij}^{a} = PL_{ij}^{a} + jQL_{ij}^{a} = V_i^{a} \times \left(I_{ij}^{a}\right)^{*} - V_j^{a} \times \left(I_{ji}^{a}\right)^{*} \tag{16}$$

$$SL_{ij}^{b} = PL_{ij}^{b} + jQL_{ij}^{b} = V_i^{b} \times \left(I_{ij}^{b}\right)^{*} - V_j^{a} \times \left(I_{ji}^{b}\right)^{*} \tag{17}$$

$$SL_{ij}^{c} = PL_{ij}^{c} + jQL_{ij}^{c} = V_i^{c} \times \left(I_{ij}^{c}\right)^{*} - V_j^{c} \times \left(I_{ji}^{c}\right)^{*} \tag{18}$$

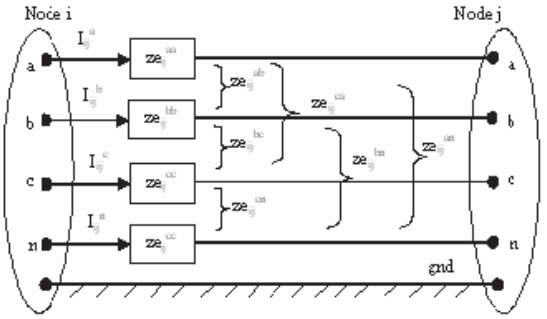

Figure.2 Three phase four wire line model

In general, the receiving end power at any phase a, of line between nodes i and j may be expressed as:

$$P_{ij}^{a} + jQ_{ij}^{a} = \left[\sum_{\substack{k=\text{index of all nodes fed} \\ \text{through the line between} \\ \text{nodes } i \text{ and } j}} \left(P_k^{a} + jQ_k^{a}\right)\right] + \left[\sum_{\substack{\text{index of all lines} \\ \text{connected between} \\ \text{nodes } m \text{ and } n \text{ fed} \\ \text{through the line} \\ \text{between nodes} \\ i \text{ and } j}} \left(P_{mn}^{a} + jQL_{mn}^{a}\right)\right] \tag{19}$$

Similarly for phases 'b' and 'c' respectively.

3. Development of Discrete Particle Swarm Optimization

Particle swarm optimization as developed by the authors comprises concept, and paradigms can be implemented in a few lines of computer code. It requires only primitive mathematical operators, and is computationally inexpensive in terms of both memory requirements and speed. Early testing has found the implementation to be effective with several kinds of problems. Particle swarm optimization has also been demonstrated to perform well on genetic algorithm test functions.

3.1 Simulating Social Behavior

One motive for developing the simulation was to model human social behavior, which is of course not identical to fish schooling or bird flocking. One important difference is its abstractness. Birds and fish adjust their physical movement to avoid predators, seek food and mates, optimize environmental parameters such as temperature, etc. Humans adjust not only physical movement but cognitive or experiential variables as well. We do not usually walk in step and turn in unison (though some fascinating research in human conformity shows that we are capable of it); rather, we tend to adjust our beliefs and attitudes to conform to those of our social peers.

3.2 Precursors: The Etiology of Particle Swarm Optimization

The particle swarm optimization is probably best presented by explaining its conceptual development. As mentioned above, the algorithm began as a simulation of a simplified social milieu. Agents were thought of as collision-proof birds, and the original intent was to graphically simulate the graceful but unpredictable choreography of a bird flock.

3.3 Nearest Neighbor Velocity Matching and Craziness

A satisfying simulation was rather quickly written, which relied on two props nearest-neighbor velocity matching and "craziness." A population of birds was randomly initialized with a position for each on a torus pixel grid and with *X* and Y velocities. At each iteration a loop in the program determined, for each agent (a more appropriate term than bird), which other agent was its nearest neighbor, then assigned that agent's *X* and *Y* velocities to the agent in focus. Essentially this simple de created a synchrony of movement.

3.4 Acceleration by Distance

Though the algorithm worked well, there was something aesthetically displeasing and hard to understand about it. Velocity adjustments were based on a crude inequality test: If presentx > bestx, make it smaller; if presentx < bestx, make it bigger. Some experimentation revealed that further revising the algorithm made it easier to understand and improved its performance. Rather than simply testing the sign of the inequality, velocities were adjusted according to their difference, per dimension, from best locations

$$vx[\ ][\ ] = vx[\ ][\ ] + rand\ (\ ) \times p\_increment \times (Pbestx\ [\ ][\ ] - presentx[\ ][\ ]) \quad (20)$$

(Note the parameters vx and presentx have two sets of brackets because they are new matrices of agents by dimensions; increment and bestx could also have a g instead of p at their beginnings.)

4. Performance of Particle Swarm Optimization Using Inertia weights

The following describes the position and velocity update equations with weight factors included.

$$V_{id} = W \times V_{id} + C_1 \times rand\ (\ ) \times (P_{id} - X_{id}) + C_2 \times Rand\ (\ ) \times (P_{gd} - X_{id}) \quad (21)$$

$$X_{id} \rightarrow X_{id} + V_{id} \quad (22)$$

Where C_1, C_2 are positive constants and called cognitive and social parameters

Equation.(21) calculates a new velocity for each particle (potential solution) based on its previous velocity, the particle's location at which the best fitness so far has been achieved, and the population global (or local neighborhood, in the neighborhood version of the algorithm) location at which the best fitness so far has been achieved. Equation.(22) updates each particle's position in solution hyperspace. The two random numbers are independently generated. The use of the inertia weight ω, which typically decreases linearly from about 0.9 to 0.4 during a run, has provided improved performance in a number of applications.

4.1 Parameter Selection in Particle Swarm Optimization

Unlike many other computational intelligence techniques, the particle swarm optimizer has few parameters to tune. Many attempts have been made to improve the performance of originally developed PSO. Many parameters have been added to the originally developed PSO to modify or to improve the performance of the technique. A quick statistical experiment is used to fine tune these parameters for the class of constrained optimization problem considered.

4.2 Swarm Size,P

The swarm size or the number of individuals inside the population is determined by the integer parameter


'P'. For very small values of P the possibility of being trapped in local optima is very likely. Larger population will increase the computation time requirements.

4.3 Number of Iterations

It is also a user defined parameter that determines the number of iterations for which algorithm has to run. Based upon computational experience a few hundred of iterations are usually sufficient to observe significant improvement in the solution providing that the initial solutions are feasible.

4.4 Velocity of Particle

One of the important factors that affect performance of the PSO, Specifically the speed of the convergence is the particle's velocity of 'flying' inside the problem space. This parameter limits the steps taken by particles at every iteration. A small value can cause the particle to get trapped in local optima; on the other hand, a too large value can cause oscillation around a certain position. This problem of proper selection of velocity can be eliminated by using adaptive velocity to PSO's position updating. The following equation represents the velocity update equation.

$$V_{id} = W \times V_{id} + C_1 \times \text{rand}(\,) \times (P_{id} - X_{id}) + C_2 \times \text{Rand}(\,) \times (P_{gd} - X_{id}) \quad (23)$$

Where c1 and c2 are positive constants, called cognitive and social parameters respectively, both are equal to 2 in general cases. 'W' is inertia weight factor; a large weight factor facilitates a global search while a small inertia weight facilitates a local search.

5. Problem formulation for Capacitor Placement

For a realistic distribution system with presence of nonlinear loads, the objective of optimal capacitor placement problem is to reduce the power loss and energy loss, and to minimize the cost of capacitor banks, while maintaining node rms voltages within prescribed values. The objective function can be expressed as

$$\min f\left(u^0, u^i\right) = k_e \sum_{i=1}^{ni} T_i P_i + \sum_{j=1}^{nc} C_j\left(u_j^0\right) \quad (24)$$

The right-hand side of equation.(24) consists of two terms. The first term represents the energy loss cost and the second term represents the total capacitor cost which comprises the purchase cost and the installment cost. Practically, capacitors are grouped in banks of standard discrete capacities (e.g., a bank of 300 kVAr); therefore, capacitor sizes are regarded as integer multiples of the standard size of one bank. To describe realistic cost of capacitor placement, the cost function of capacitors at node j is

$$C_j\left(u_j^0\right) = k_{inst} + k_{cj}\frac{u_j^0}{u_s} \quad (25)$$

Where k_{inst} is a constant representing a fixed installment cost of capacitor banks; k_{cj} is the purchase cost of one capacitor bank: $k_{cj} = k_{cf}$ for fixed capacitor banks and $k_{cj} = k_{cs}$ for switched capacitor banks with $k_{cf} < k_{cs}$. The cost function $C_j\left(u_j^0\right)$ is a non-differentiable and piece-wise function as illustrated in Figure.4. Consequently, the capacitor placement problem is a non-linear mixed integer optimization problem with non-differentiable objective function that cannot be efficiently solved by conventional optimization techniques.

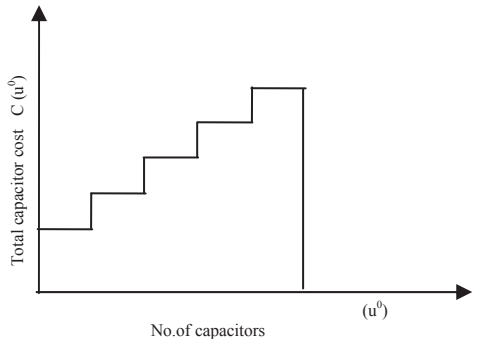

Figure.4 The cost functions of capacitor banks.

5.1. Illustrations of Candidate Node Identification

The proposed node identification method is explained with 15- node system. After running the load flows for base case system, the active power loss is given by 60.34821 kW. By compensating reactive power injection at every node equal to local reactive load, one at a time and perform the load flows and calculate the active power loss in each case and also loss reductions. The results are tabulated in Table 1. The most suitable nodes for capacitor placement are chosen based on the condition PLI greater than a PLI tolerance value between '0' and '1'. The tolerance value is selected by experimenting with different values in descending order starting from '1'. The best value of the tolerance is the value which gives the highest profit and satisfying the system constraints. The Power Loss Indices (PLI) are calculated as

$$PLI_{[i]} = \frac{(\text{lossreduction}[i] - \text{minimumreduction})}{(\text{maximum reduction} - \text{minimumreduction})} \quad (26)$$

5.1.1 Algorithm for Node Identification

Following algorithm explains the methodology to identify the candidate nodes, which are more suitable for capacitor placement.

- Read radial distribution system data.


- Run the load flows and calculate the base case active power loss.
- By compensating the reactive power injections (Q_c) at each node and run the load flows, to calculate the active power losses in each case.
- Calculate the power loss reduction and power loss index using equation(26).
- Select the candidate node whose PLI>Tolerance.
- Stop.

Table 1 Power loss reductions

Node no	Power loss after compensation Q_c at each node (kW)	Loss Reduction (kW)
2	58.948	1.4005
3	56.982	3.3665
4	53.078	7.2704
5	57.876	2.4719
6	57.376	2.9721
7	58.41	1.9379
8	54.54	5.8081
9	55.311	5.0368
10	57.587	2.761
11	52.916	7.4327
12	56.124	4.2246
13	57.563	2.7856
14	56.425	3.9236
15	52.835	7.5129

Table 2 The power loss indices 15 node system

Node no	PLI
2	0.0000
3	0.3216
4	0.9603
5	0.1753
6	0.2571
7	0.0879
8	0.7211
9	0.5949
10	0.2226
11	0.9869
12	0.4620
13	0.2266
14	0.4128
15	1.0000

6. Results and Analysis

The proposed method is illustrated with two different cases as follows.

Case-I: Illustrates the capacitor placement of balanced 15-node radial distribution system.

Case-II: Illustrates the capacitor placement of un-balanced 19-node radial distribution system.

Case-I: The proposed algorithm is tested on 15-node radial distribution system. The line and load data are given in ref [9]. The power loss index (PLI) tolerance of 0.5 is chosen to get maximum profit as shown in Table.3. The results of 15-node radial distribution system at different load levels before and after compensation by using fixed and switched capacitors are given in Table 4. The summary of test results is given in Table 5.The voltage profile before and after compensation are shown in Figure 4. From the results, it is observed that active power losses reduce from 60.34821 kW to 29.77601kW i.e., 50.6596 % loss reduction and minimum voltage improved from 0.942389 p.u to 0.967561 p.u. thus voltage regulation improved from 5.7611% to 3.2439%, i.e., 43.6930 % improved.

Table.3 Total profit in a year for different PLI tolerance values

PLI tolerance	No. of candidate nodes	Candidate nodes	Total profit (Rs)
0.9	3	4, 11, 15	900751.81
0.7	4	4, 8, 11, 15	964803.12
0.5	**5**	**4, 8, 9, 11, 15**	**979106.14**
0.3	8	3, 4, 8, 9, 11, 12, 14, 15	947228.68
0.1	12	3, 4, 5, 6, 8, 9, 10, 11, 12, 13, 14, 15	343391.37

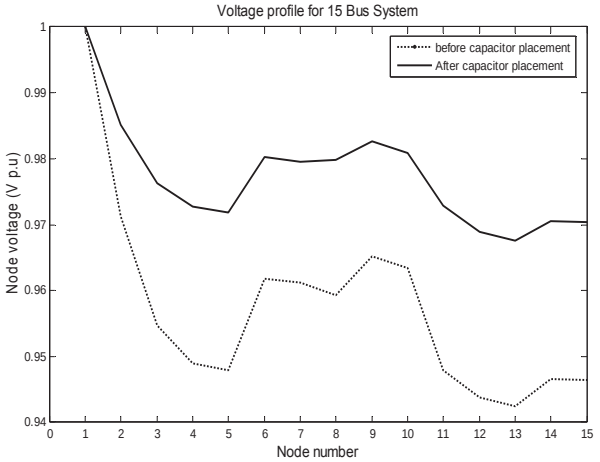

Figure.4 Voltage profile for 15-node system before and after compensation for full load

Table.4 Test Results of 15-Node System at different load levels before and after Compensation

Load level	Capacitors (kVAR)		Total Losses (kW)		Minimum Voltage (p.u)	
	Fixed	Switched	Before Compensation	After Compensation	Before Compensation	After Compensation
0.5	$Q_{C(4)}$= 0	$Q_{C(4)}$= 300	14.346233	9.357631	0.971951	0.979091
	$Q_{C(8)}$=0	$Q_{C(8)}$=0				
	$Q_{C(9)}$=0	$Q_{C(9)}$=0				
	$Q_{C(11)}$=0	$Q_{C(11)}$=0				
	$Q_{C(15)}$=0	$Q_{C(15)}$=0				
1.0	$Q_{C(4)}$= 0	$Q_{C(4)}$= 300	60.348211	29.776017	0.942389	0.967561
	$Q_{C(8)}$=0	$Q_{C(8)}$=300				
	$Q_{C(9)}$=0	$Q_{C(9)}$=300				
	$Q_{C(11)}$=0	$Q_{C(11)}$=300				
	$Q_{C(15)}$=0	$Q_{C(15)}$=0				
1.2	$Q_{C(4)}$= 0	$Q_{C(4)}$= 0	88.774877	44.877899	0.930082	0.955847
	$Q_{C(8)}$=0	$Q_{C(8)}$=300				
	$Q_{C(9)}$=0	$Q_{C(9)}$=300				
	$Q_{C(11)}$= 0	$Q_{C(11)}$= 300				
	$Q_{C(15)}$=0	$Q_{C(15)}$=300				

Table.5 Summary of results of 15 node system before and after compensation for load level of '1' p.u

Description	15-node system		33-node system	
	Before Compensation	After Compensation	Before Compensation	After Compensation
Total reactive Power load (kVAR)	1251.17	51.17	2300	1100
Reactive power loss	59.3422	28.9419	135.239381	96.375501
Released reactive power Demand (kVAR)	-----	1230.4003	-----	1238.863880
Real power losses (kW)	60.348211	29.776017	202.706961	143.725587
Loss reduction (%)	-----	50.6596	-----	29.096866
Real power Demand(kW)	1286.7482	1256.17601	3917.706961	3858.725587
Released demand (kW)	-----	30.572194	-----	58.981374
Feeder Capacity (kVA)	1836.6173	1258.7279	4612.896993	4039.935333
Released feeder capacity (kVA)	-----	577.8893	-----	572.961661
Min.voltage (p.u)	0.942389	0.967561	0.913041	0.925082
Voltage regulation (%)	5.7611	3.2439	8.6959	7.4918
Improvement of Voltage regulation (%)	-----	43.6930	-----	13.8468
Power cost (Rs)	1730786.69	1033976.17	5813635.63	4302049.82
Net savings (Rs)	-----	696810.52	-----	1511585.81

Case-II: The proposed algorithm for unbalanced radial distribution system is tested on 19-node radial distribution system. The line and load data of 19 node radial distribution system are given ref [7]. The summary of test results of 19-node radial distribution system is given in Table.6. From the results, it is observed that total active power losses reduce from 13.473 kW to 11.257 kW i.e., 16.443 % loss reduction and minimum voltage of phase A, phase B and phase C improved from 0.95159, 0.94975, 0.95046 p.u to 0.95751, 0.95572, 0.95641 p.u. respectively. The voltage profile for phase A, phase B and phase C before and after compensation are shown in figure.5., figure.6 and figure.7. respectively.

7. Conclusion

A Discrete Particle Swarm Optimization for Optimal Capacitor Placement in Radial Distribution System has been proposed in this paper. With full considerations of different load levels, and practical aspects of fixed or switched capacitor banks, the target problem is reformulated by a comprehensive objective function and a set of equality and inequality constraints. The proposed solution method employs PSO to search for optimal locations, types, and sizes of capacitors to be placed and optimal numbers of switched capacitor banks at different load levels.

An effective approach for optimum location of capacitor in radial distribution system has been proposed. From the results, several important observations can be concluded as follows.

- The power losses of distribution system can be efficiently reduced by proper placement of capacitor.
- In addition of power loss reduction, the voltage profile can be improved as well by the proposed method.


Table.6 Summary of test result of 19-node system before and after compensation

Description		19-node system	
		Before Compen sation	After Compen sation
Q_C required (kVAR)		90.000	……..
Total reactive Power load (kVAR)		183.066	101.113
Released reactive Power (kVAR)		……..	81.953
Min.Voltage (p.u)	PhaseA	0.95159	0.95751
	PhaseB	0.94976	0.95572
	PhaseC	0.95046	0.9565
Voltage Regulation (%)	PhaseA	4.8408	4.2486
	PhaseB	5.0242	4.44281
	PhaseC	4.9534	4.3591
Improvement of Voltage regulation	Phase A	……..	12.2335
	PhaseB	…….	11.5717
	PhaseC	……..	11.9978
Total losses (kW)		13.473	11.258
Loss reduction (%)		……	16.443
Demand (kW)		379.413	377.198
Released demand (kW)		……	2.215
Feeder capacity (kVA)		421.268	390.515
Released Feeder Capacity(kVA)		…….	30.753
Net savings (Rs)		……	38012.06

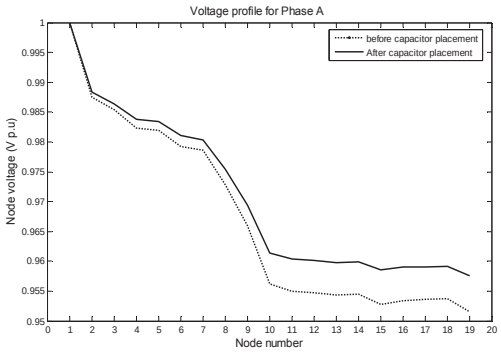

Figure.5.Voltage profile for Phase A

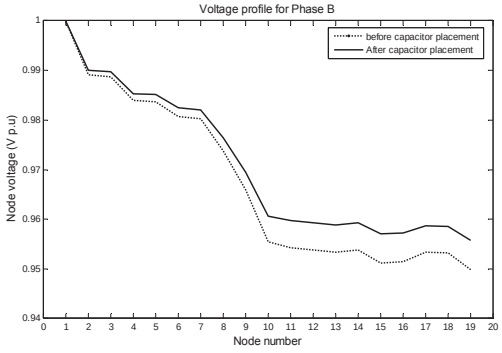

Figure.6. Voltage profile for Phase B

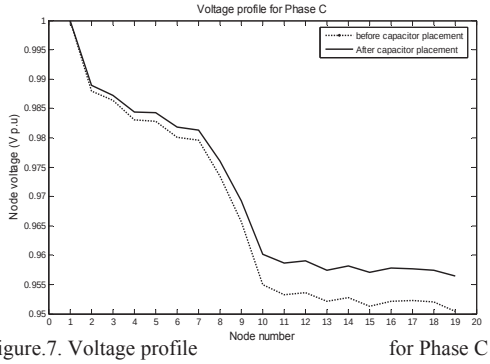

Figure.7. Voltage profile for Phase C

8. References

[1] Nelson E.Change, "Generalised equation on loss reduction with shunt capacitors", IEEE Trans.PAS, Nov. 1971, pp.2189-2195.

[2] M.E.Baran and F.F.Wu, "Optimal capacitor placement on distribution systems" IEEE Trans.on Power Delivery, Vol. 4, January 1989, pp. 725-734.

[3] M.E.Baran and F.F.Wu, "Optimal sizing of capacitor placed on a radial distribution systems" IEEE Trans.on Power Delivery, Vol. 4, January 1989, pp. 735-743.

[4] Srinivasaan Sundharajan, Anil Pahaw, "optimal selection of capacitors for radial distribution systems using genetic algorithm, IEEE Transaction on Power systems, Vol9, No.3, August 1994.

[5] J.Kennedy, R.Ebehart, " Particle Swarm Optimization" in Procedings of the 1995 IEEE,International Conference on Neural Networks, Vol 4,pp1942-1948.

[6] J.Kennedy,"The particle Swarm: Social adoption of knowledge" IEEE, 1997. James Kennedy, "Small words and mega minds, Effects of neighborhood trpology on particle swarm performance", IEEE 1999.

[7] D.Thukaram, H.M.Wijekoon Banda and Jovitha Jerome, " A robust three phase power flow algorithm for radial distribution systems" Electric Power Systems Research, November 11, 1998.

[8] Xin-me Yu, Xin-yin Xiong, Yao-wu Wu, " A PSO-based approach to optimal capacitor placement with harmonic distortion consideration", Electric Power Systems Research, January 2004.

[9] D.Das, et.al., "Noval Method for solving the RadialDistribution Networks" Proc.Int.Conf, Vol 141, No.4, July 1994, pp 291-298.

[10] M.H.Shwehdi,A.Mantawi,et.al "Capacitor Placement in distribution systems,A new formulation"IEEE Bologna Power Tech Conference,June23-26,2003.

[11] G.Carpinelli,P.Varilone,et.al "Capacitor Placement in three phase distribution systems with nonlinear and Unbalanced loads"IEEPorc-Gene, Tran,Dist, Vol 152, No.1, January 2005.

Biographies

J.Viswanatha Rao obtained his B.Tech degree in Electrical & Electronics Engineering from J.N.T.University in 1997.He obtained his M.Tech degree in Electrical power system from J.N.T.University.He is working as an Associate Professor in the department of Electrical and Electronics Engineering in Swarnandhra College of Engineering and Technology.Narsapur-534275.His areas of interest are Power systems, Electrical Distribution Systems,Particle Swarm Optimization application to Distribution Systems.

Dr.S.Sivanagaraju received his Masters degree in 2000 from IIT, Kharagpur and did his Ph.D from J.N.T.University in 2004.He is currently working as associate professor in the department of Electrical Engineering. J.N.T.U.College of Engg. (Autonomous) Anantapur, Andhra Pradesh,India. He had received two national awards (Pandit Madan Mohan Malaviya memorial prize award and Best paper prize award) from the institute of engineers(India) for the year 2003-04.He is referee for IEE Proceedings-Generation Transmission and Distribution and International journal of Emerging Electrical Power System.He has 40 publications in National and International journals and conferece to his credit. His areas of interest are in Distribution Automation,Genetic Algorithm application to distribution systems and power system.

www.icgst.com

AN IMPROVED QUASI-SLIDING MODE CONTROL STRATEGY

C.Vivekanandan, R. Prabhakar, M. Gnanambigai
Department of Electrical and Electronics Engineering, Coimbatore Institute of Technology, Avanashi Road, Civil Aerodrome Post, Coimbatore – 641 014, India.
vivekanandan.cit@gmail.com, rpcitpr@gmail.com, ambika323@yahoo.com
http://www.cit.edu.in

Abstract
Discrete sliding mode control (DSCM) is one of the best techniques in analyzing the dynamics of nonlinear systems. This paper presents an improved discrete quasi-sliding mode control strategy in which the control input for the next step is determined by considering the dynamics of the current disturbance, which improves the robustness of the system dynamics with relatively smaller control effort. In fact, the existing techniques fail to deliver satisfactory response for parameter variations and time-varying external disturbances, where as the complete robustness is guaranteed in the proposed technique. This improved strategy is applied to two different systems under various environmental conditions and the results obtained demonstrate its effectiveness and improved efficiency.

Key Words**:** *Variable-structure system, discrete time system, quasi sliding-mode, state-space.*

1. Introduction
Variable structure control (VSC) is a general approach for the design and control of a class of nonlinear systems. VSC is implemented along with the stochastic control techniques like fuzzy logic, neural networks to obtain better dynamics [1]. In variable structure control the system is allowed to vary its structure by properly and deliberately changing the sign and / or magnitude of the input, forcing discontinuities in the input with respect to time. The plane which separates these different structures is called as switching plane or switching surface. This discontinuous input makes the phase trajectory of the system to undergo two modes, *reaching mode* and *sliding mode*. In reaching mode, the system phase trajectory, starting from anywhere on the phase plane moves toward a switching plane and reaches it in finite time. This is followed by sliding mode in which the phase trajectory asymptotically tends to the origin of the phase plane [6], [8], [9]. The switching surface decides the closed loop dynamics of the system which are at the designer's choice and hence, also known as sliding mode control (SMC). The main advantage of SMC is its insensitivity to parameter variations, external disturbances and modeling errors [6], [9].

With the advent of digital computers and its widespread use in control systems, considerable efforts have been put in the study of discrete time VSC/SMC techniques, called as discrete sliding mode control techniques (DSMC) [2], [3], [6]. In discrete sliding mode the control input is constant over sampling periods. Hence, when the states reach the switching surface, the subsequent control would be unable to keep the states to be confined to the surface. This leads the system to undergo only quasi-sliding mode, i.e., the system states would approach the sliding surface but would generally be unable to stay on it [6]. Thus, DSMC does not posses the invariance property found in continuous time sliding mode.

Gao introduced '*reaching law*' method to design the controller for continuous-time VSC [4] and extended the same for discrete time counterpart [3]. This approach is found satisfactory when compared to the other methods proposed in [5]. The switching function $s(k)$ is effectively controlled to meet the required dynamics and also to satisfy the constraints of DSMC. This is followed by the derivation of the control law in conjunction with the known plant model and parameter variations.

The technique proposed by Gao is simpler and directly deals with the reaching process and makes it easy to obtain the control law [4]. However, chattering in the steady state is a major drawback, which is due to the discontinuous switching control applied to the plant, which excites the unmodelled high frequency dynamics of the system.

Bartoszewicz proposed a state-feedback-based control law for uncertain systems with *bounded uncertainties* that guarantee's discrete sliding mode [2]. This is an improved version of Gao's method and ensures finite time convergence of phase trajectories on the sliding plane without chattering. However, this method is effective only for systems with time invariant external disturbances. For systems with parameter uncertainties and time varying external disturbances this technique fails to deliver satisfactory results as the system becomes unstable or stable with steady-state errors.

By redefining the *priori* known function defined in [2], it is found that this technique requires lesser control effort, but still unsuitable for systems influenced by parameter variations and external disturbances. In this paper a redefined discrete quasi-sliding mode control strategy based on Bartoszewicz's control law for *unbounded and time varying uncertainties* is proposed. The modified technique not only improves the robustness of the system dynamics, but also requires smaller control effort compared to the previous strategies, while retaining the finite time convergence of the state trajectory to the sliding surface.

The paper has been organized into six Sections. Section 2 gives an overview of DSMC and reaching condition details. Bartoszewicz technique is briefly discussed in Section 3 along with the redefined version of it. Section 4 explains the new improved quasi-sliding-mode control strategy for an uncertain system with unbounded uncertainties and the details of the two numerical examples considered in this paper. The responses of the example systems under different conditions and the improvements in the system dynamics and efficiency are discussed in Section 5. Section 6 provides the conclusion and future work.

2. Discrete Quasi-Sliding Mode and Reaching Conditions

A. Preliminaries:
Consider a discrete-time system represented by,

$$\begin{aligned} \boldsymbol{x}(k+1) &= \boldsymbol{A}\boldsymbol{x}(k) + \Delta\boldsymbol{A}\boldsymbol{x}(k) + \boldsymbol{b}u(k) \\ &\quad + \boldsymbol{f}(k) \\ y(k) &= \boldsymbol{h}^{\boldsymbol{T}}\boldsymbol{x}(k) \end{aligned} \tag{1}$$

where $\boldsymbol{x}$ is the $n \times 1$ state vector, $\boldsymbol{A}$ is an $n \times n$ system matrix, $\boldsymbol{b}$ and $\boldsymbol{h}$ are input and output vectors of appropriate dimensions, u is the system input, and y is the system output. The pair $(\boldsymbol{A}, \boldsymbol{b})$ must be controllable. Further, the $n \times n$ parameter variation matrix $\Delta\boldsymbol{A}$ and the $n \times 1$ external disturbance vector $\boldsymbol{f}$ satisfy the matching conditions [6],

$$\Delta\boldsymbol{A} = \boldsymbol{b}\bar{\boldsymbol{A}} \qquad \bar{\boldsymbol{A}} \text{ - a row vector}$$

$$\boldsymbol{f} = \boldsymbol{b}\bar{\boldsymbol{f}} \quad \bar{\boldsymbol{f}} \text{- scalar}$$

Define the switching function

$$s(k) = \boldsymbol{c}^{\boldsymbol{T}}\boldsymbol{x}(k) \tag{2}$$

with vector $\boldsymbol{c}$ such that $\boldsymbol{c}^{\boldsymbol{T}}\boldsymbol{b} \neq 0$ and the resulting quasi-sliding motion is stable. Disturbances and parameter variations are bounded, so that the following relation holds:

$$d_l \leq d(k) = \boldsymbol{c}^{\boldsymbol{T}}\Delta\boldsymbol{A}\boldsymbol{x}(k) + \boldsymbol{c}^{\boldsymbol{T}}\boldsymbol{f}(k) \leq d_u \tag{3}$$

where the lower bound d_l and the upper bound d_u are known constants and $d(k)$ is the disturbance vector. Further more define $d_0 = 0.5(d_l + d_u)$ and $\delta_d = 0.5(d_u - d_l)$, where d_0 the average is value of $d(k)$ and δ_d is the maximum possible deviation as shown in Figure.1. The quasi-sliding mode is defined as the motion such that $|s(k)| \leq \epsilon$, where the positive constant ϵ is called the quasi-sliding-mode bandwidth.

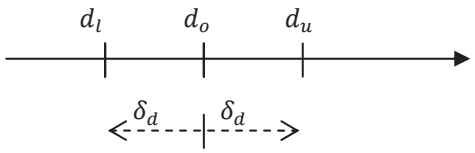

Figure.1. Deviation of $d(k)$

B. Reaching condition and reaching mode:
The condition under which the system states starting from any initial state, move towards the sliding surface and reach it in finite time, called as *reaching condition* or *reaching law*. The system trajectory under the reaching condition is called the *reaching mode* or *reaching phase*. So, under ideal conditions there exists a finite time t_e such that for all $t \geq t_e$, the sliding function $s(x) = 0$.

In continuous time the reaching law is a differential figure which specifies the dynamics of a switching function $s(x)$. A simple reaching law may be written as [4]

$$\frac{ds}{dt} = -q\ (sgn(s)) \tag{4}$$

In the above condition the parameter q decides the rate of convergence of $s(x)$ towards the sliding surface and the magnitude of chattering in the sliding mode. Hence, by proper choice of the parameter q in (4), the dynamic quality of VSC system in the reaching mode can be controlled.
In case of discrete mode the condition given in (4) is written as

$$s(k+1) - s(k) = -qT\left(sgn\big(s(k)\big)\right) \quad (5)$$

where T is the sampling period. The condition specified by (5) assures that

$$|s(k+1)| < |s(k)| \quad (6)$$

However, this condition fails to ensure the finite time convergence. Hence, the objective is to determine a suitable function that steers the system to sliding surface in finite sampling period. Gao in [3] suggested a condition

$$s(k+1) - s(k) = -qT\big(sgn(sk)\big) - \epsilon T s(k)$$
$$\epsilon > 0,\ q > 0 \text{ and } 1 - \epsilon T > 0$$

which results in chattering and its magnitude is limited with in the so called quasi-sliding mode bandwidth (QSMB), given by

$$2\Delta = 2\frac{qT}{1-\epsilon T}; \quad (7)$$

Bartoszewicz suggested a new reaching law [2]

$$s(k+1) = d(k) - d_0 + s_d(k+1) \quad (8)$$

where $s_d(k)$ is a *priori* known function. In this technique the system state is steered to the sliding plane $s(k) = 0$, and do not allowed cross it, and hence, chattering is eliminated and ideal quasi-sliding mode can be achieved for certain systems. Following section gives a brief overview of this technique.

3. Bartoszewicz's Reaching Law

A. Fundamentals:

Bartoszewicz proposed a reaching law, given in (8) in which the unknown $d(k)$ is defined by (3) and $s_d(k)$ is an a *priori* known function such that the following applies [1].

[1]
If $s(0) > 2\delta_d$, then (9)
$s_d(0) = s(0)$
$s_d(k).s_d(0) \geq 0$, for any $k \geq 0$
$s_d(k) = 0$, for any $k \geq k^*$
$|s_d(k+1)| < |s_d(k)| - 2\delta_d$, for any $k < k^*$.

[2] Otherwise, i.e., if $s(0) \leq 2\delta_d$, then $s_d(k) = 0$ for any $k \geq 0$.

The constant k^*, in relations (9), is a positive integer chosen by the designer in order to achieve good trade-off between the fast convergence rate of the system and the magnitude of the control u required to achieve this convergence rate. The definition chosen in [2] for $s_d(k)$, when $s(0) > 2\delta_d$ is

$$s_d(k) = \frac{k^*-k}{k^*}s(0)$$
$$k^* < \frac{s(0)}{2\delta_d} \quad (10)$$

where $k = 0,1,\cdots,k^*$.

In order to determine the control u which drives the system in such a way that the reaching law (8) is satisfied, (1) and (2) are used to calculate $s(k+1)$:

$$s(k+1) = \boldsymbol{c^T A x}(k) + \boldsymbol{c^T}\Delta \boldsymbol{A x}(k) + \boldsymbol{c^T b}u(k) + \boldsymbol{c^T f}(k)$$
$$s(k+1) = \boldsymbol{c^T A x}(k) + d(k) + \boldsymbol{c^T b}u(k) \quad (11)$$

Comparing this figure with the reaching law (8), the following is obtained.

$$s_d(k+1) - d_0 = \boldsymbol{c^T A x}(k) + \boldsymbol{c^T b}u(k) \quad (12)$$

Hence, the input is given by

$$u(k) = -(\boldsymbol{c^T b})^{-1}[\boldsymbol{c^T A}x(k) + d_0 - s_d(k+1)] \quad (13)$$

By this means, a control law is designed, which guarantees that, for any $k \geq k^*$, the system state satisfies the following inequality:

$$|s(k)| = |d(k-1) - d_0| \leq \delta_d \quad (14)$$

B. Redefined Bartoszewicz law:

Let the *priori* known function given in (10) be redefined as [10]

$$s_d(k) = \frac{k^*-k}{k^*}\boldsymbol{s(k)} \quad (15)$$

The redefined law is applied to the same example considered in [2] with $k^* = 12$, and simulated for 100 samples, i.e. $k = 100$. The control effort computed with redefined method is $\boldsymbol{J = 611.0295}$, and that of from original technique is $\boldsymbol{J = 682.3333}$, which shows the improvement in the redefined method.

4. Improved Quasi-Sliding Mode Control Strategy

The technique discussed above is effective only for systems with bounded and known uncertainties. For systems with time invariant external disturbances the techniques discussed above exhibit ideal sliding mode characteristics and fail to deliver satisfactory dynamics when the system is subjected to parameter uncertainties and / or time varying disturbances. Hence, the following modifications are made to overcome these difficulties.

Let the reaching law (8) be redefined as

$$s(k) = s_p(k) \quad (16)$$


where $s_p(k)$ is *a prior* known function. The definition chosen for $s_p(k)$ in this paper is

$$s_p(k) = \frac{k_f - k}{k_f} s(k) \tag{17}$$

The constant k_f is a suitable positive integer chosen by the designer at which the system states would converge exactly to the sliding surface after k_f time samples without chattering, and effectively bringing down the quasi-sliding mode band to zero. The constrains defined in (9) are redefined as follows

$$\begin{aligned} &\text{If } s(0) \neq 0, \text{ then} \\ &s_p(0) = s(0) \\ &s_p(k).\, s_p(k-1) \geq 0, \quad \text{for any } k \geq 0 \\ &\left|s_p(k+1)\right| < \left|s_p(k)\right|, \quad \text{for any } k < k_f. \\ &s_p(k) = 0, \quad \text{for any } k \geq k_f \end{aligned} \tag{18}$$

The above constrains assure the sliding mode for systems given by (1). Comparing (11) and (17) and solving for $u(k)$, the redefined control law is given as

$$u(k) = -(\boldsymbol{c^T b})^{-1}[\boldsymbol{c^T A}x(k) + d(k) - s_p(k+1)] \tag{19}$$

The above input $u(k)$ ensures ideal sliding mode and finite-time convergence for both parameter variations and time varying external disturbances. Hence, the controllers, designed using the proposed method, are highly robust and it is also found a relatively lesser control effort is required to achieve this improved dynamics.

In Bartoszewicz technique the transition from reaching mode to sliding mode is sharp and abrupt where as in the proposed technique the transition is smooth. Due to this, a discontinuity in the system output is avoided and hence an improved system dynamics is achieved. This leads to relatively better output quality and lesser control effort than the same required in Bartoszewicz technique.

NUMERICAL EXAMPLES:

EXAMPLE-I:
To prove the effectiveness of the modified reaching law, a system with following parameters is considered [2].

$$\boldsymbol{A} = \begin{bmatrix} 1 & 1 \\ 0 & 0.5 \end{bmatrix}; \quad \boldsymbol{b} = \begin{bmatrix} 0 \\ 1 \end{bmatrix} \text{ and } \quad \boldsymbol{h} = \begin{bmatrix} 1 \\ 0 \end{bmatrix};$$

The sliding line considered is $c^T = [1 \quad 1]$ and the initial condition assumed is $\boldsymbol{x}(0) = [1000 \quad 0]^T$. The values taken for k_f and k are set to 12 and 100 respectively. With the above assumptions the system is simulated under four different environments and the results obtained are discussed in detail in the next section.

EXAMPLE-II:
The system considered in [7] is chosen as the second example to demonstrate the advantages of the proposed technique over the existing technique. The parameters of this system are as follows.

$$\boldsymbol{A} = \begin{bmatrix} 0 & 1 \\ 0.4 & -0.3 \end{bmatrix}; \quad \boldsymbol{b} = \begin{bmatrix} 0 \\ 1 \end{bmatrix} \text{ and } \boldsymbol{h} = [1 \quad 0]$$

In this example the parameter variation and the external disturbances are lumped together and given as

$$d(k) = \begin{bmatrix} 0 \\ \left(\sin\left(\frac{k}{2}\right)\right)\left(\exp\left(-\frac{k}{5}\right)\right) \end{bmatrix}$$

The sliding line is taken as $\boldsymbol{c}^T = [-0.4 \quad 1]$ and the initial condition is $\boldsymbol{x}(0) = [10 \quad 0]^T$. This system is also simulated with both existing and proposed techniques and the advantages of the latter are discussed in the next section. For both examples the required control effort is calculated as $\boldsymbol{J} = \sum_{k=0}^{100} |u(k)|$ and output quality factor is computed as $\boldsymbol{Q} = \sum_{k=0}^{100} |y(k)|$.

5. Results and Discussion

Example I - Case I:
In this case, the system given in example-1 is subjected to a time invariant external disturbance and without parameter variations, i.e. $\Delta\boldsymbol{A} = 0$ and the external disturbance vector considered is $\boldsymbol{f}(\boldsymbol{k}) = [0 \quad 1]^T$, same as in [2]. The system is simulated and the responses of $s(k)$ and $y(k)$ are presented in Figure 2.a and Figure 2.b respectively. It is clear from the plots that, with the proposed method the system dynamics are smooth and settles early and void of steady state error.

Example I - Case II:
For the same system referred in *Case-I*, the following parameter variation $\Delta\boldsymbol{A}$ is introduced and simulated.

$$\Delta\boldsymbol{A} = \begin{bmatrix} 0 & 0 \\ 1 & 1 \end{bmatrix}$$

The responses of $s(k)$ and $y(k)$ are plotted in Figure 3.a and Figure 3.b respectively. It is obvious that the system is unstable with the existing method and perfectly stable with the proposed method.


Example I - Case III:
For the system given in example-1, the following time varying external disturbance is included

$$\begin{bmatrix} f_1 \\ f_2 \end{bmatrix} = \begin{bmatrix} 0 \\ 0.04 * |50 - k| - 1 \end{bmatrix}$$

With no parameter variations, i.e. $\Delta A = 0$ the system is simulated and the response curves are plotted in Figure 4.a1, Figure 4.a2, Figure 4.b1 and Figure 4.b2, which clearly show the improved robustness in the proposed.

Example I - Case IV:
The system is subjected to both parameter variation and time varying external disturbance with their values set same as before. The dynamics of $s(k)$ and $y(k)$are plotted in Figure 5.a and Figure 5.b. The system is found stable with the controller designed using the proposed method and highly unstable with its existing counterpart.

Example - II:
The system described in example-II is simulated using both Bartoszewicz technique and proposed technique and the responses are plotted in Figure 6.a and Figure 6.b. The steady state error present in the Bartoszewicz technique is eliminated.

Table-1 and Tabel-2 summarize the control efforts and output quality factors respectively, measured under different conditions for both examples with Bartoszewicz technique and the technique proposed in this paper. It is obvious that the proposed technique results in better output quality with a relatively lesser input control effort. Irrespective of the presence of the external disturbances and/or parameter variations the system is stable with the controllers designed using proposed technique and hence the proposed technique is more efficient and robust.

For different choices k_f the control effort is measured for both *Example-I (Case-I)* and *Example-II* and plotted in Figure.7 and Figure.8, which demonstrates the better efficiency in the proposed method than in the existing technique.

6. Conclusion:

In this paper the redefined and the modified discrete-time sliding mode strategies based on the techniques proposed by Bartoszewicz are presented. It is found that the redefined technique presented in this paper is better efficient but fails to deliver satisfactory system dynamics for systems with parameter variations and external disturbances, as in the case of existing technique. The modified technique proposed in this paper guarantees complete robustness for both parameter variation and time varying external disturbances. In addition, this is achieved at reduced control effort, leading to better and efficient performance, while retaining the relaxed constraints of quasi-sliding mode. The improvement in the performance is proved by simulating two different case studies under various conditions. The simulation is done for SISO systems and can easily be extended for MIMO systems also.

7. References

[1] Ahmed Belhani, Fateh Mehazem and Khaled Belarbi. 'Decentralized backstepping controller for a class of nonlinear multivariable systems', ICGST International Journal on Automatic Control and Systems Engineering, ACSE, Vol.6., No.2, pp. 41-48, 2006.

[2] Bartoszewicz A. 'Discrete-time quasi-sliding-mode control strategies', IEEE Trans. Ind. Electron., Vol.45, no.4, pp.633-637, Aug.1998.

[3] Gao W. B., Wang Y., and Homaifa A. 'Discrete-Time Variable Structure Control Systems', IEEE Trans. Ind. Electron., Vol.42, No.2, pp.117-122, Apr 1995.

[4] Gao W. B. and Hung J. C. 'Variable structure control of nonlinear systems: A new approach', IEEE Trans. Ind. Electron, Feb.1993, pp. 45-55.

[5] Govert Monsees 'Discrete-Time Sliding Mode Control', Ph.D. Thesis, ISBN 90-77017-83-6, 2002.

[6] Hung J. Y., Gao W. B., and Hung J.C. 'Variable structure control: A survey', IEEE Trans. Ind. Electron., Vol.40, No.1, pp.2-21, Feb 1993.

[7] Janardhanan S. and Bandyopadhyay B. 'Output feedback sliding-mode control for uncertain systems using fast output sampling techniques', IEEE Trans. Ind. Electron., Vol.53, No.5,October 2006.

[8] Utkin V. I, 'Variable structure systems with sliding mode', IEEE Trans. Autom. Control, Vol. AC-22, No.2, pp.212-222, Apr 1977.

[9] Utkin V. I. 'Sliding Modes and Their Applications in Variable Structure Systems', Moscow, Nauka, Mir, 1978.

[10] Vivekanandan C., Prabhakar R. and Gnanambigai M. 'A redefined quasi-sliding mode control strategy', Proceedings of World Academy of Science, Engineering and Technology, Volume 29, pp 292-295, May 2008, Issn: 1307-6884.

Table-1
Comparison of the total control effort
$\boldsymbol{J} = \sum_{k=0}^{100}|u(k)|$ Computed for different strategies

Strategy	*Example-1*				*Example-2*
	Case I	*Case II*	*Case III*	*Case IV*	
Bartoszewicz	682.33	**Unstable**	633.33 (with modified Bartoszewicz technique)	**Unstable**	48.5768
Proposed	**611.03**	**4.64e3**	**563.86**	**4.64e3**	**17.8702**

Table-2
Comparison of the output quality factor
$\boldsymbol{Q} = \sum_{k=0}^{100}|y(k)|$ Computed for different strategies

Strategy	*Example-1*				*Example-2*
	Case I	*Case II*	*Case III*	*Case IV*	
Bartoszewicz	7500	**Unstable**	7504.10 (with modified Bartoszewicz technique)	**Unstable**	56.8044
Proposed	**5036**	**5036**	**5042.20**	**5036**	**21.8313**

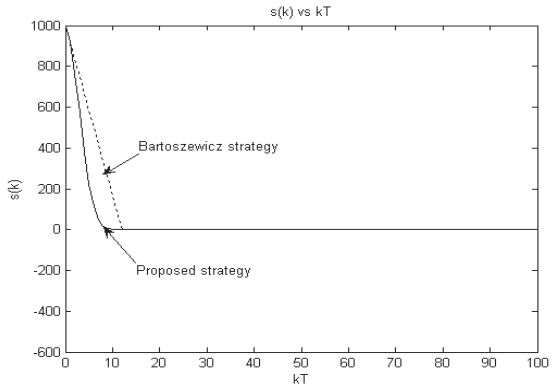

Figure 2.a

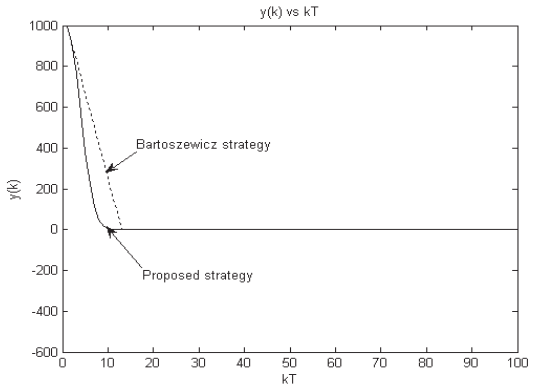

Figure 2.b

Figure.2. Response of switching function $s(k)$ and output $y(k)$of system with time invariant disturbance *Example1_Case I*

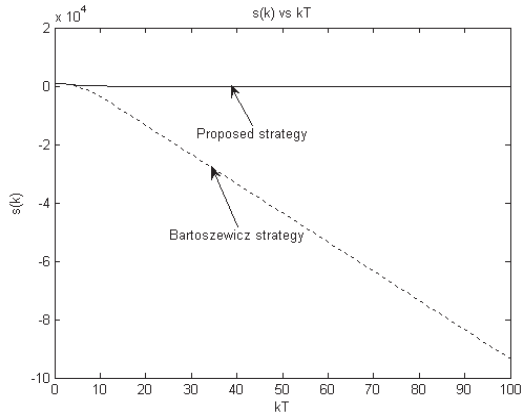

Figure 3.a

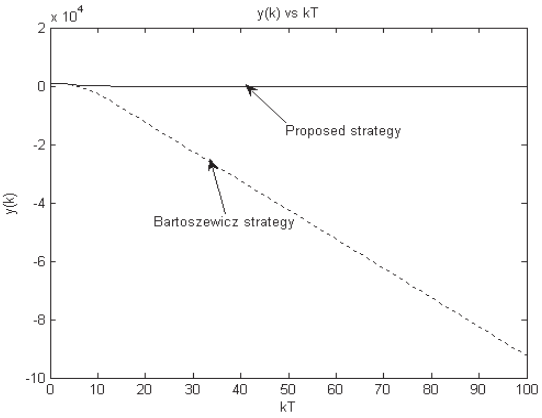

Figure 3.b

Figure.3. Response of switching function $s(k)$ and output $y(k)$of system with parameter variation *Example1_Case II*

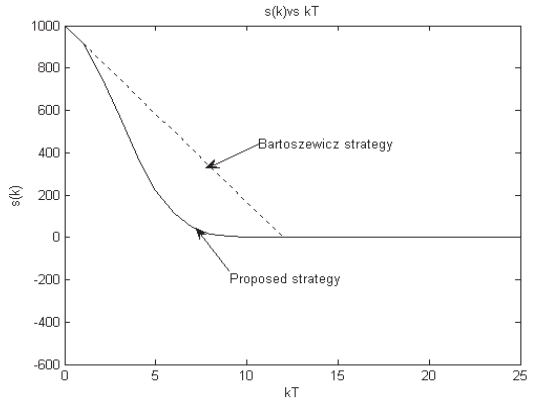

Figure 4.a1

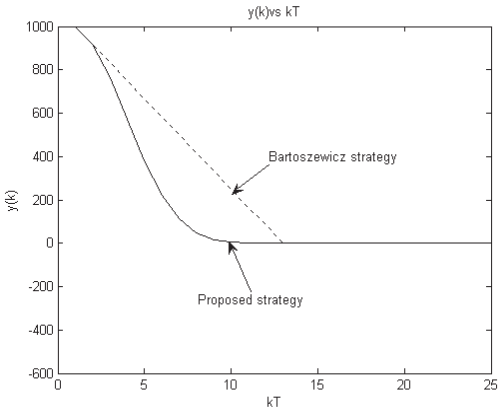

Figure 4.b1

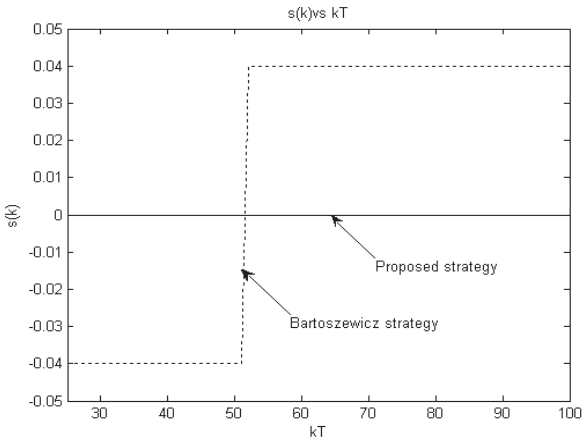

Figure 4.a2

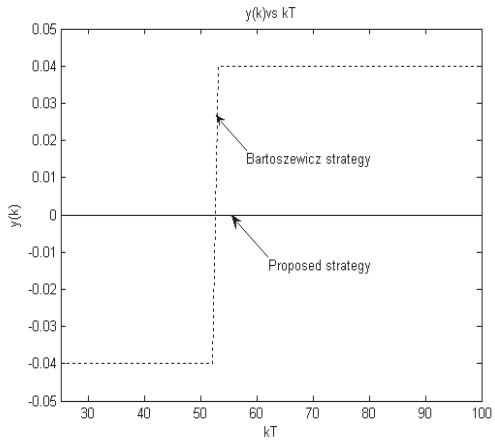

Figure 4.b2

Figure.4. Response of switching function $s(k)$ and output $y(k)$of system with time varying disturbance *Example1_Case III*

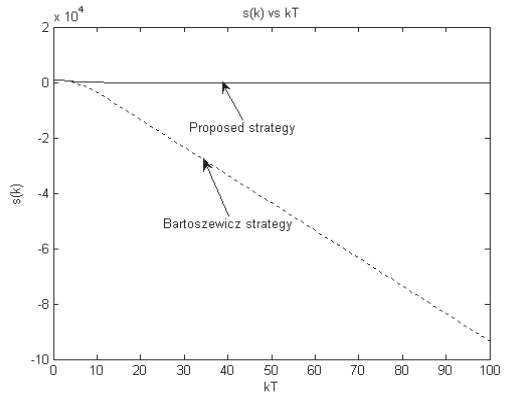

Figure 5.a

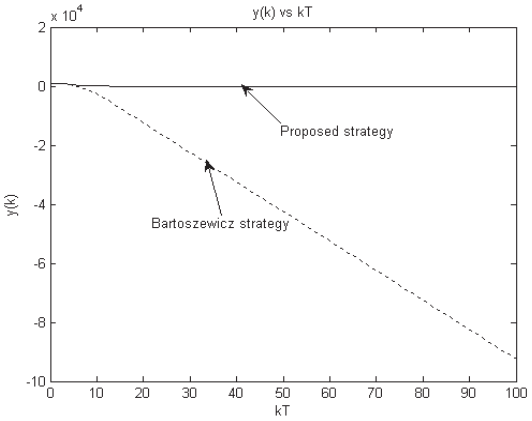

Figure 5.b

Figure.5. Response of switching function $s(k)$ and output $y(k)$of system with time varying disturbance and parameter variation *Example1_Case IV*

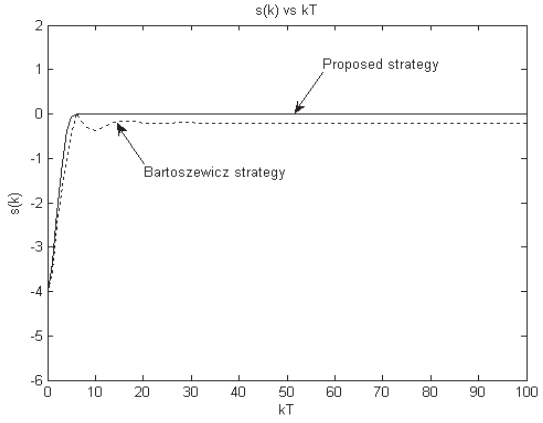

Figure 6.a

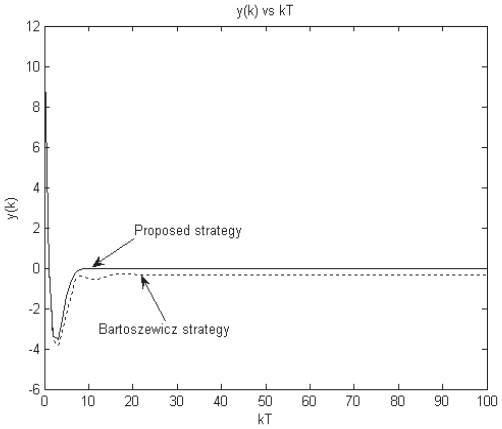

Figure 6.b

Figure.6. Response of switching function $s(k)$ and output $y(k)$of system with lumped parameter variation and external disturbance *Example2*

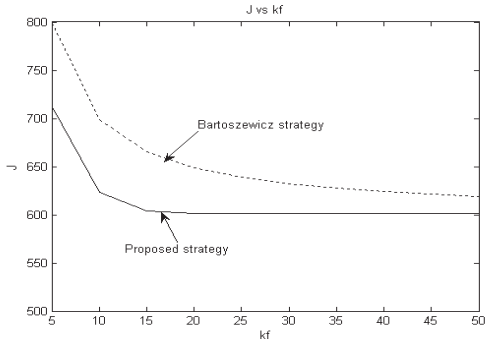

Figure.7. Control effort $\boldsymbol{J}$ required for different $\boldsymbol{k_f}$ *Example 1*

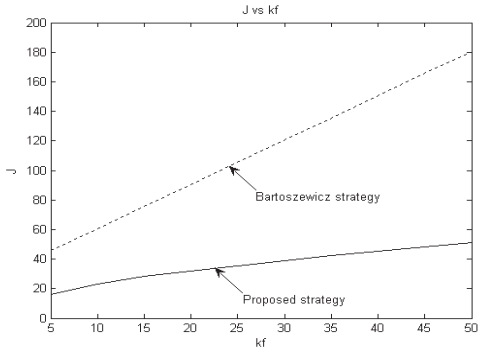

Figure.8. Control effort $\boldsymbol{J}$ required for different $\boldsymbol{k_f}$ *Example 2*

Biographies

C. Vivekanandan received the B.E. Degree in Electrical and Electronics Engineering from Bharathiar University, Coimbatore, Tamilnadu, India in 1986 and the M.E. Degree in Applied Electronics from the same university in 1988. Presently he is pursuing his research in the area of digital control systems under Anna University, Chennai, India. He is working a Selection Grade Lecturer in the Department of Electrical and Electronics Engineering, Coimbatore Institute of Technology, Coimbatore, Tamilnadu, India. His areas of interest are Control Systems, Microprocessor based system design and algorithm developing.

Contact:

Mr. C. VIVEKANANDAN
Selection Grade Lecturer,
Department of Electrical and Electronics Engineering
Coimbatore Institute of Technology
Coimbatore, Tamilnadu, India – 641 014.
Phone: +919443720312
Email: vivekanandan.cit@gmail.com

Dr. R. Prabhakar obtained his B. Tech. degree in Mechanical Engineering from IIT- Madras, Chennai, Tamilnadu, India and M.S. degree from Osmania State University, USA. He received his Ph.D. from Purdue, USA. He is a member of several national and international technical societies. He was the syndicate member of Anna University. He has a number of national and international publications to his credit. Presently he is the Head of Coimbatore Institute of Technology, Coimbatore, India.

Contact:

Dr. R. Prabhakar,
Principal,
Coimbatore Institute of Technology,
Coimbatore Institute of Technology
Coimbatore, Tamilnadu, India – 641 014.
Phone: +91422 2574071
Email: rpcitpr@gmail.com

Ms. Gnanambigai obtained her B.E. degree in Electrical and Electronics Engineering from Anna University, Chennai, India in 2005 and pursuing her M.E. degree in Applied Electronics. Her areas of interest are feedback control system and digital design.

Contact:

Ms. M. Gnanambigai
Research Assistant,
Department of Electrical and Electronics Engineering
Coimbatore Institute of Technology,
Coimbatore, Tamilnadu, India – 641 014.
Phone: +919940495286
Email: ambika323@yahoo.com

www.icgst.com

An Explicit Solution for the Optimal Control of Greenhouse Temperature relying on Embedded System

I. Laribi Maatoug, R.Mhiri
I.N.S.A.T de Tunis, Département Génie physique et Instrumentation
B.P.N°676,1080-Tunis Cedex- Tunisie Tel : (+216.71)703829
ibtissem.maatoug@planet.tn
Radhi.Mhiri@planet.tn

Abstract

This paper presents an "explicit predictive control" with optimal performances of the heating system in a greenhouse. The main contribution of this work is to provide an offline solution of modeling and optimization in order to implement the control over a simple micro-controller without the need for computer. Based on a multi-model description of the temperature in a greenhouse, we represent this system in the Mixed Logical Dynamical (MLD) form using the modeling language (HYSDEL); once the MLD model of the system is determined, the equivalent Piecewise Affine (PWA) model is generated directly. The optimal control profile is a piecewise affine and continuous function based on a PWA model and an Explicit Model Predictive Controller , the aim of this control is to keep the temperature into a defined range, and in the same time reducing consumption and optimizing the number of switching of the heating control. Simulations with the proposed approach are presented and compared to the existing control; the results indicate a reduction of consumption between 17 and 44% according to the value of external temperature while the correspondent number of switching remains in acceptable margins

Keywords: *Agricultural Greenhouse, Predictive control, Hybrid modeling: MLD and PWA, Predictive control, optimal control.*

1. Introduction

In the Mediterranean environment, a greenhouse requires the control of the climate in order to maintain the agricultural environment in appropriate conditions that satisfy the agronomic and economic objectives of the farmer, hence the relevance of approaching this problem from an optimization point of view. The predictive control with optimal performances has been recently used in some greenhouses, reader can refer to [1] and [2]; the first work using a hybrid representation (MLD) was published in 2008 [3]. The advantage of the current work is to have an offline optimal control directly in the "ON/OFF" form (constraint of the heating equipment) and the optimization of the switching number. To achieve the design of efficient controllers for the greenhouse, we need to develop models that describe efficiently the system to be simulated and controlled. These models must be related to the experimental influence of outside parameters such as air temperature, wind speed, etc...In the case of our greenhouse, the four controls are working separately, so we have independent subsystems. In this paper we suggest to model and control the temperature under the action of the heating system. This sub-system is non linear with time-varying parameters[4], that's why we represent it with the multi-model approach in order to decrease the complexity of the whole system, and to provide an interesting alternative to the method of the online identification which is the most used in the control of greenhouses [5]. This multi-model representation and the on/off nature of the heating control give the model a hybrid nature; the characteristic of these systems is the interaction between continuous-time dynamics (governed by differential equations), and discrete dynamics and logic rules (described by temporal logic, finite state machines, if-then-else conditions, discrete events, etc.) and discrete components (on/off switches, selectors, digital circuitry, software code, etc.). We focus here on a particular case of discrete-time hybrid systems: the mixed logical dynamical systems (MLD) introduced by Bemporad and Morari [6] and the piecewise affine systems PWA by Sontag [7]. Based on multi-model description of the temperature inside an agriculture greenhouse, we first model this system in the MLD form using the HYSDEL language; once the MLD model is available, the equivalent PWA model is generated automatically using appropriate algorithm. By modeling our system in the PWA form, we are going to develop the explicit solution (in the offline mode) of a predictive control based on the reducing of consumption and the optimization of number of switching of the heating system. The explicit form of the Model Predictive Control offers an alternative route to an efficient controller implementation, opening up the route to use

MPC in fast and cheap systems where the on-line solution is prohibitive; especially in the case of greenhouses where the environment is not suited for installation and maintenance of computers.

The remainder of the paper is organized as follows: Section (2) presents the greenhouse system and the existing heating control .Section (3) presents the temperature modelling in multimodel, MLD and PWA form. Section (4) summarizes basic knowledge of MPC strategy control associated with PWA models. Section (5) presents the explicit solution of optimal control applied to the case of the greenhouse. Experimental results are reported in section (6). Finally the conclusion and the scope of further work are provided in section (7).

2. Greenhouse description

This application concerns an experimental greenhouse, located at the "Institut National de la Recherche Scientifique et Technologique (INRST)" at Borj Cedria area, a suburb 20 kms south of Tunis. The experiment consists in developing an acquisition station and climatic control. It involves a group of hardware and software which permit the acquisition and numerical storage of the climatic data such as: temperature, humidity, solar radiation and wind speed. The control system uses a personal computer. The measured values are continuously stored in the computer; the control algorithm switches on or off the appropriate systems in order to control different parameters (temperature, humidity, etc...) [8], [9] to develop a model of the temperature, we consider an input/output data of the process with different perturbation as illustrated in figure 1:

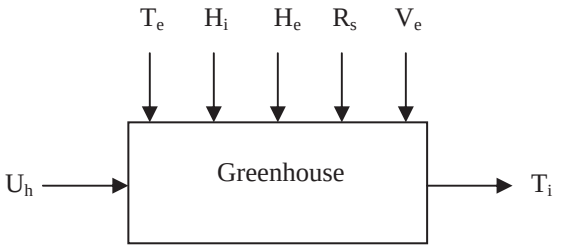

Figure 1. Input/output Diagram

Where:

T_i : Inside Temperature.
H_i : Inside Humidity: measured disturbance
T_e : Outside Temperature: measured disturbance
H_e : Outside Humidity: measured disturbance
Ve : Wind speed: measured disturbance
R_s : Solar radiation: measured disturbance
U_h : Heating control

The existing heating control: The existing heating control works according to the following principle: If the internal temperature Ti decreases less than 18°C, the heating control is activated and it remains active until Ti exceeds 20°C, the heating is stopped and will be reactivated only if Ti decreases less than 18°C [7]. This system is subject to constraints in the inside temperature of greenhouse (viability constraint: $18°C \le T_i \le 20°C$) and control inputs (ON/OFF nature of the heating control) [4] This control gives the following curve of temperature (figure.2):

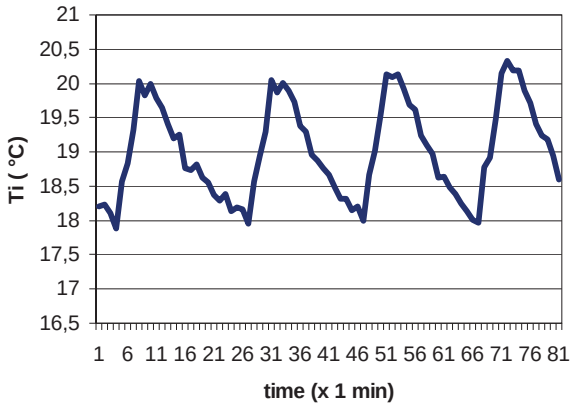

Figure 2. Inside temperature under existing heating control

3. Modeling temperature under the greenhouse

The linearization of the model around a functioning point ends in the following system of state space equations [9]:

$$T_i(k) = a_1 T_i(k-1) + a_2 T_i(k-2) + a_3 T_i(k-3) + a_4 U_h(k-1) + a_5 T_e(k-1) + a_6 H_i(k-1) + a_7 H_e(k-1) + a_8 R_s(k-1) + a_9 V_e(k-1) \quad (1)$$

Where k is the discrete time-instant

Multimodel approach: The multimodel approach is interesting as it describes complex process by a set of linear models which constitute library of models. Each model represents a partial, local, and/or simplified description of the process. The choice of the models library needs a good physical knowledge of the process and its environment. The process can be described by the models M1, M2... Mn, with D1, D2... Dn, domain of validity of each model. If the domains of validity are separated then coefficients v1, v2... vn can take only values 0 or 1 and verify in each instant the following relation: v1+v2+...+vn=1. In this approach we have studied 18 measurements related to March and May 2003. These measures covered a large variation of external temperature in Tunisia from 0°C to 18°C by night and day. Based on a human expertise, we found for each range of external temperature the model Mi that describes it to the better (Table.1). The multi-model approach used is based on the method of separated domains validity. The validation of the multi-model approach is verified on about thirty measurement sets between years 1999 to the year 2003. This study allowed us to arise 5 functioning zones; each one is characterized by a distinct model [9]:

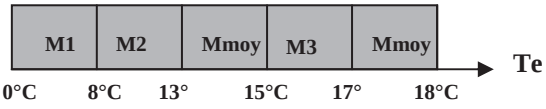

Figure 3. Multimodel description according to different value of external temperature

Table 1 Parameters of Models

	a_1	a_2	a_3	a_5
M1	1,026	0,1883	-0,3575	0,0732
M2	0,9982	0,2815	-0,3757	0,0466
Mmoy	0,8704	0,2843	-0,2197	0,04315
M3	0,8189	0,3111	-0,1766	0,0475
	a6	a7	a8	a9
M1	-0,0132	0,0735	-0,0003	0,0082
M2	0,045	-0,0093	0,0015	0,0019
Mmoy	0,0064	0,008	0,0003	0,0067
M3	-0,0114	0,0108	0,0019	0,0051

Remark: a_4= 0.6 for the 4 models

Mixed Logical Dynamical (MLD) representation: The Mixed Logical Dynamical (MLD) framework is a powerful tool for modelling discrete-time linear hybrid systems. Its main favorable feature is its ability to model logical parts of processes and heuristics knowledge about plant operation as integer linear inequalities. The general MLD form of a hybrid system is:

$$\begin{aligned} x(k+1) &= Ax(k) + B_1 u(k) + B_2\delta(k) + B_3 z(k) \\ y(k) &= Cx(k) + D_1 u(k) + D_2\delta(k) + D_3 z(k) \\ E_2\,\delta(k) + E_3 z(k) + E_5 &\le E_4 x(k) + E_1 u(k) + E_5 \end{aligned} \quad (2)$$

Where k is the discrete time-instant, and x(k) denotes the states, u(k) the inputs and y(k) the outputs, with both real and binary components. Furthermore, delta and z represent binary and auxiliary continuous variables, respectively. All constraints on states, inputs, outputs and auxiliary variables are summarized in the mixed-integer linear inequality constraint. The MLD framework allows for convenient modeling using the Hybrid Systems Description Language HYSDEL developed by Torrisi [10], [11].

HYSDEL Language: When modeling a hybrid system of any realistic degree of complexity, appropriate tools are required to efficiently and efficaciously represent and describe the model dynamics in an adequate formal setup. In this sense HYSDEL provides an intuitive textual interface for modeling a class of hybrid systems described by interconnections of linear dynamic systems, automata, if-then-else and propositional logic rules. Hysdel translates the given description into the MLD form. The resulting MLD model can be immediately used for optimization, to solve, e.g., optimal control problems, a simulator of the model can be generated as a function in Matlab. A HYSDEL list is made of two parts INTERFACE and IMPLEMENTATION. The INTERFACE section contains the declarations, divided into subsections called STATE, INPUT, OUTPUT and PARAMETER. The second part, IMPLEMENTATION, is made of specialized sections describing the relationships among the variables; this part starts with an optional AUX section which contains the system internal signals declarations. The OUTPUT section allows specifying static linear and logic relationships for the output vector. The section AD allows defining Boolean variables from continuous ones. The section DA defines continuous variables according to if-then-else conditions on Boolean variables. The section LOGIC allows specifying arbitrary functions of Boolean variables. The CONTINUOUS section describes the linear dynamics. The LINEAR section allows defining a continuous variable as an affine function of continuous variables. And finally The MUST section specifies constraints on continuous and Boolean variables. For a more detailed description of the syntax and the functionality of the HYSDEL modelling language and the associated compiler (HYSDEL tool) the reader is referred to [11],[12]

Modeling greenhouse temperature in the MLD form: Obtaining the PWA form from a Multimodel representation is very difficult when we work with systems presenting a high number of entries and states. This has led us to use the MLD form equivalent to the PWA one and easy to obtain by using the HYSDEL programming language.

In order to have a predictive controller optimizing consumption and the number of switching $|U_h(k) - U_h(k-1)|$, we need two MLD models of the greenhouse.

The first one considers the measured disturbances (external temperature and humidity, wind speed, solar radiation and inside humidity) like inputs. The value of $U_h(k-1)$ is stored in an additional state.

The first MLD hybrid model generated from the HYSDEL file <greenhouseplant.hys> is composed of:

4 states (4 continuous, 0 binary)
6 inputs (5 continuous, 1 binary)
1 outputs (1 continuous, 0 binary)
22 continuous auxiliary variables
21 binary auxiliary variables
142 mixed-integer linear inequalities

The second one associate with the controller consider the measured disturbances like additional states; the value of $U_h(k)$ is stored in an additional output.

The second MLD hybrid model generated from the HYSDEL file <greenhousextend.hys>is composed of:

8 states (8 continuous, 0 binary)
1 inputs (0 continuous, 1 binary)
2 outputs (1 continuous, 1 binary)
21 continuous auxiliary variables
21 binary auxiliary variables
140 mixed-integer linear inequalities

The HYSDEL code for the "greenhouseplant" is given in Appendix.

Piecewise Affine (PWA) representation: Polyhedral PWA systems are defined by partitioning the input-state space into polyhedral and associating with each polyhedron an affine state-update and output function, that is:

$$\begin{aligned} x(k+1) &= A_i x(k) + B_i x(k) + f_i \\ y(k) &= C_i x(k) + D_i u(k) + g_i \qquad if \begin{bmatrix} x(k) \\ u(k) \end{bmatrix} \in \chi_i \end{aligned} \quad (3)$$

$$(x(k), u(k)) \in \chi_i = \left\{ (x,u) \,\middle|\, F_i x + G_i u \le K_i \right\} \quad (4)$$

where u(k), x(k) and y(k) respectively represent the input, state and output of the system at time k and all matrices A_i, B_i, C_i, D_i ,and vectors f_i, g_i contain real entries and are of appropriate dimension. The set χ_i defines the polyhedral partition in the state-input space as shown in the figure.4 , Fi , Gi are guard lines of the partition χ_i and define constraints on state and input variables .

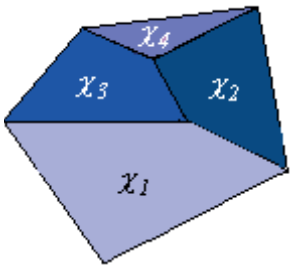

Figure 4. Piecewise affine systems

In other words, a PWA description is suitable for a system that evolves according to different dynamics depending on the specific point in the state-input space under consideration. PWA systems are the object of extensive research because they constitute an immediate extension of linear systems capable of modeling nonlinear/non-smooth phenomena with an arbitrary degree of precision and they allow considering fundamental hybrid features such as linear-threshold events and mode switching [7].

Modeling greenhouse temperature in the PWA form: For a given well-posed MLD model there always exists an *equivalent* PWA representation. Equivalence implies that for all feasible initial states and for all feasible input trajectories, both models yield the same state and output trajectories. The conversion from MLD to PWA form is performed efficiently using an enumeration algorithm [13], [14]. The two PWA models generated from the MLD one are defined over 25 polyhedral regions, with the same number of Input, state and output of the respective MLD models.

4. Predictive control of hybrid system

Model predictive controller: Model predictive control (MPC) has proved it's efficiently in controlling a wide range of applications in industry; the reader will refer to [15] for examples .MPC is able to control a great variety of processes, including systems with long delay times, non-minimum phase systems, unstable systems, multivariable systems, and constrained systems. The main idea of predictive control is the use of a plant model to predict future outputs of the system. Based on this prediction, at each sampling period, a sequence of future control values is elaborated through an on-line optimization process. Only the first value of this sequence is applied to the plant, the whole procedure is repeated again at the next sampling period according to the 'receding' horizon strategy .The cost function to be minimized is generally a weighted sum of square predicted errors and square future control values [16].

Explicit Model Predictive control: For PWA systems, we can design optimal and sub-optimal control laws either in implicit form, where an optimization problem of finite size is solved on-line in a Receding Horizon Control manner or, alternatively, solve an optimal control problem in a multi-parametric fashion and an explicit representation of the control law is obtained [17],[18].

By using multi-parametric mathematical programming, the closed-form of the optimal control law can be computed off-line for the whole admissible range of the system states. The resulting feedback controller inherits all the stability and performance properties of MPC, no on-line LP solver is needed in the MPC implementation, which requires only the evaluation of a piecewise affine function. The optimal control problem is defined as follows:

$$\min_U J(U,x,r) = \sum_{k=0}^{N-1} \left\| R(y(k)-r) \right\|_p + \left\| Qu(k) \right\|_p$$
$$subject\ to \begin{cases} PWA\ mod\ el \\ x(0)=x \end{cases} \tag{5}$$

The MPC controller is piecewise affine in x,r :

$$u(x,r) = \begin{cases} F_1 x + E_1 r + g_1 & if \quad H_1 \begin{bmatrix} x \\ r \end{bmatrix} \le K_1 \\ \vdots & \vdots \\ F_M x + E_M r + g_M & if \quad H_M \begin{bmatrix} x \\ r \end{bmatrix} \le K_M \end{cases} \tag{6}$$

Where x and r respectively represent the state and the output reference, Fi, Ei, gi, and H_i, K_i defines the polyhedral partition in the state-reference space (figure.5). The solution u(x, r) can be found via a combination of Dynamic programming or enumeration of feasible mode sequences and multi-parametric linear or quadratic programming and polyhedral computation [19],[20]

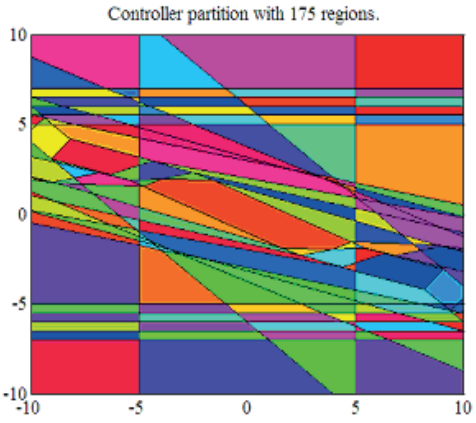

Figure 5. Example of Controller partition in the (x,r) space

5. Optimal control of greenhouse temperature: the explicit controller

Cost function: Our goal is to keep the temperature into the interval [18, 20°], and in the same time to minimize the heating control consumption and the number of switching, we chose the following cost function:

$$J_N = \sum_{k=1}^{N-1} Q_u U_h(k) + Q_y \left| U_h(k) - U_h(k-1) \right| \quad (7)$$

The first term design the control consumption, with U_h is an on/off control (equal to 1 or 0), the second term design the number of switching and equal to the absolute value of the difference between $U_h(k)$ and $U_h(k-1)$, Qy and Qu ; are weights on input and number of switching. The two criteria 'number of switching' and 'consumption' are opposite, we can't increase one without decreasing the other one; our cost function looks then for the equilibrium between these two criteria. The result obtained with the cost function (7) is not interesting; the algorithm of optimization gives us only two results: either the control giving optimal consumption, or the control minimizing the number of switching, whatever the values of N or weights. To improve these results we introduced another term in the cost function in order to find the control minimizing the two previous criteria; This new criterion is the term minimizing the difference between the output and a fixed reference (equal to 19°C) corresponding to the middle of viability interval [18, 20 ° C]. The new cost function is:

$$J_N = \sum_{k=1}^{N-1} Q_u U_h(k) + Q_{y1} \left| y(k) - y_{1ref} \right| + Q_{y2} \left| U_h(k) - U_h(k-1) \right| \quad (8)$$

In this approach, we don't have the constraint related to the time computation, since obtaining the inputs/states partition is made offline; so the choice of the value of the prediction horizon is linked to the results obtained and the number of regions produced which grows exponentially with the value of N (for N=2 we have 83 regions, for N=3 we have 550, for N=4 we have 4069 regions). So we choose the small value of N (N= 2).

After several tests, the best results correspond to the following values of weight: Qu=1.6, Qy_1=1, Qy_2=1; the correspondent Explicit MPC controller is defined over 83 regions in 10 dimensions.

Controller design: We design an explicit controller in the offline mode with the two PWA models; the corresponding optimal solution was computed with the MPT toolbox developed by Kvasnica [21]. We treat as hard constraints upper and lower bounds on the output.

6. Results and discussion

To simulate the studied approach, we consider the nights belonging to each of the zones defined by the multi-model representation, figure.3.

Remark: All the figures present only duration of 50 minutes in order to show clearly the trajectories of internal temperature with the optimal and existing control.

Region with model M1: In this region with external temperature < 8°C, we simulate the approach with measures of the night of 18/03 for a total duration of 714 minutes.

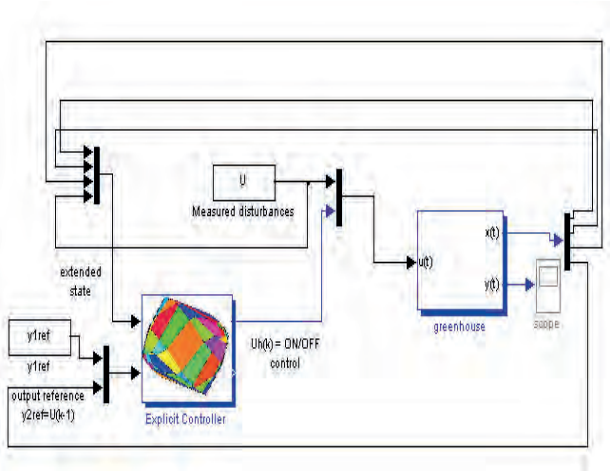

Figure 6. Explicit controller of the heating system

Table 2 Performances of Explicit controller and existing control: night 18/03

night: 18/03	Sum Uh consumption minutes)	=Sum Ns= (inswitching number	average inside temperature
Explicit control	306	192	18.71°C
Existing Control	376	113	18.99°C

For a consumption gain of 18.6%, the number of switching is increased by 1.7 times; the average of the inside temperature decreased by 0.28 ° C.

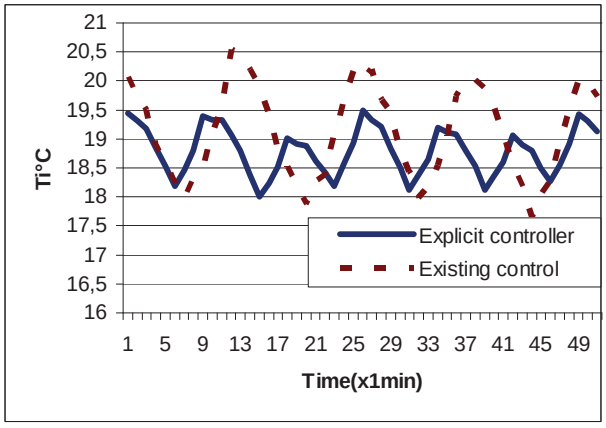

Figure 7. Inside temperature night 18/03

Region with model M2: In this region with external temperature between 8°C and 13°C, we simulate the approach with measures of the night of 16/05 for a total duration of 430 minutes.

Table 3 Performances of Explicit controller and existing control: night 16/05

night: 16/05	Sum Uh consumption (in minutes)	=Sum Ns= switching number	average inside temperature
Explicit control	96	71	18.77°C
Existing Control	113	49	19.06°C

For a consumption gain of 15%, the number of switching is increased by 1.4 times; the average of the inside temperature decreased by 0.29 ° C.

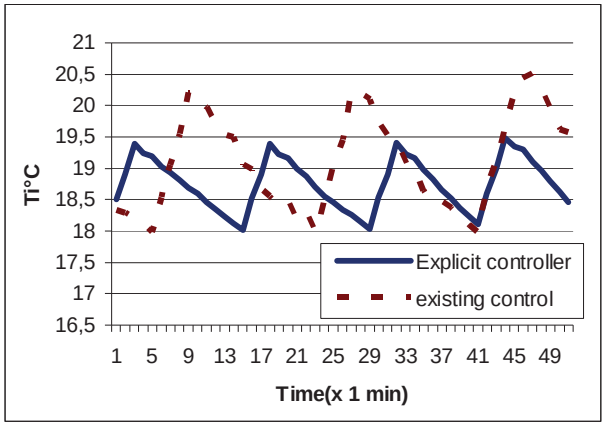

Figure 8. Inside temperature night 16/05

Region with model Mmoy: In this region with external temperature in the interval [13°C,15°C] or [17°C, 18°C], we simulate the approach with measures of the night of 21/05 for a total duration of 130 minutes.

Table 4 Performances of Explicit controller and existing control: night 21/05

Cold night: 21/05	Sum Uh consumption (in minutes)	=Sum Ns= switching number	average inside temperature
Explicit control	10	9	18.57°C
Existing Control	18	7	18.92°C

For a consumption gain of 44%, the number of switching is increased by 1.28 times; the average of the inside temperature decreased by 0.35 ° C.

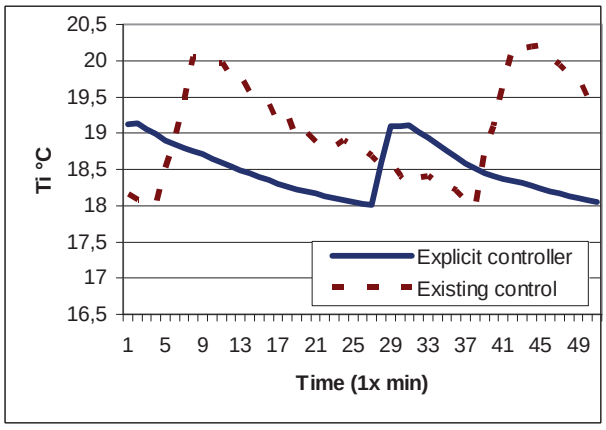

Figure 9. Inside temperature night 21/05

Region with model M3: In this region with external temperature between 15°C and 17°C, we simulate the approach with measures of the night of 29/05 for a total duration of 452 minutes.

Table 5 Performances of Explicit controller and existing control: night 29/05

night: 16/05	Sum Uh consumption (in minutes)	=Sum Ns= switching number	average inside temperature
Explicit control	52	44	18.60°C
Existing Control	80	35	19.01°C

For a consumption gain of 35%, the number of switching is increased by 1.25 times; the average of the inside temperature decreased by 0.41 ° C.

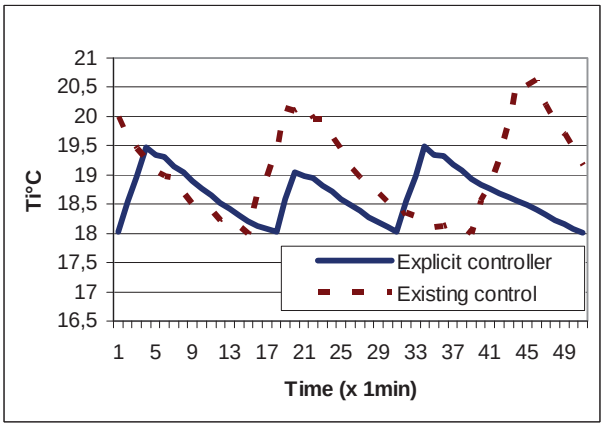

Figure10. Inside temperature night 29/05

Discussion: We noticed a reduction in the heating consumption more important (between 35% and 44%) for the warm nights (21 and 29 May with external temperature more than 13°C) than for the cold nights of 18 March and 16 May where the external temperature is lower than 13°C (between 15% and 18.6%). The number of switching stays in acceptable margins: for the cold nights it increased by 1.4 and 1.7 times comparing to the existing control; for the warm nights it increased by 1.25 and 1.28 times. The Explicit controller treats the viability constraint (inside temperature operating in the interval [18, 20 °C]) as a hard constraint; so, contrary to the existing control, the internal temperature has never been out of this interval, because the predictive controller anticipates and applies the appropriate control before the temperature falls below 18 ° C or exceeds 20 ° C.

7. Conclusion

In this paper we have described a hybrid model and an explicit controller with optimal performances for a greenhouse system. The key feature of this approach is the simultaneous optimization of the consumption and the switching number of the ON/OFF heating control in the offline mode. Based on a multimodel description of the greenhouse system, we developed two Hybrid models MLD and PWA taking into account, the measured disturbances, and getting the previous value of the heating control. Once the PWA representation of the greenhouse is available, we obtain the closed-form of the optimal control law computed in an offline mode. The

results obtained with the optimal control are interesting particularly in term of reducing consumption. In fact we obtained a reduction of heating consumption between 17% and 44%; the correspondent switching number remains in acceptable margins. The proposed approach can be applied for further industrial applications in order to reduce consumption and preserve the control equipment while taking into account uncontrollable disturbances. Its biggest advantage is the ability to be implemented on a microcontroller, which is much more suited for industrial conditions, and for people who are not necessarily familiar with the use of computers. The proposed approach will be applied in future works, to the other sub-systems of the greenhouse such as cooling and ventilation.

8. References

[1] J.P Coelho, P.B de Moura Oliveira and J. Boaventura Cunha . Greenhouse air temperature predictive control using the particle swarm optimisation algorithm. Computers and Electronics in Agriculture p 330–344 . 2005

[2] R.J.C Ooteghem,, G. van Straten and L.G Willigenburg. Receding horizon optimal control of a solar greenhouse In: Book of abstracts of the 25th Benelux Meeting on Systems and Control 2006

[3] F. Rodrıguez,, J.L Guzman, M. Berenguel, and R. Arahal . Adaptive hierarchical control of greenhouse crop production. International Journal of Adaptive Control Signal Processing. 2008, VOL 22, pages 180-197

[4] J. Boaventura Cunha , J. P. de Moura Oliveira. optimal management of greenhouse environments EFITA 2003 Debrecen,Hungary

[5] J. Boaventura Cunha, C. Couto, and A.E.B Ruano. Real-time parameter estimation of dynamic temperature models for greenhouse environmental control. Control Eng. Practice.Journal Code: 123, vol. 5, no. 10, pp. 1473-1481, 1997.

[6] A. Bemporad,, M. Morari. Control of Systems Integrating Logic, Dynamics, and Constraints. Automatica 35(3), 407-427. (1999)

[7] E.D Sontag . Nonlinear regulation: the piecewise linear approach. IEEE Trans Aut Control, 26(2):346-357(1981)

[8] M. Souissi, M. Annabi. Commande par logique floue du climat d'une serre agricole ENTROPIE, n°229,pp.24-30,(2001)

[9] I. Laribi , R. Mhiri. Modeling of a greenhouse temperature: comparison between multimodel and neural approache , ISIE06 Monréal, Canada

[10] A. Bemporad. Hybrid Toolbox for real time applications User.s Guide. April 2006

[11] F.D Torrisi, A. Bemporad and D. Mignone Hysdel a tool for generating hybrid models. Technical report, Automatic control laboratory, ETH Zuerich. 2003

[12] http://control.ee.ethz.ch/~hybrid/modeling.php

[13] A. Bemporad . A Recursive Algorithm for Converting Mixed Logical Dynamical Systems into an Equivalent Piecewise Affine Form . IEEE Trans. Autom. Control. 2003

[14] W.P.M.H. Heemels, B. De Schutter and A. Bemporad Equivalence of hybrid dynamical models Automatica 37(7):1085–1091, 2001

[15] A. Vivas, V. Mosquera. Predictive functional control of a PUMA robot . ACSE 05 Conference, 19-21 December 2005, CICC, Cairo, Egypt

[16] E.F Camacho, C. Bordons Model Predictive Control. Advanced Textbooks in Control and Signal Processing.. Springer, 2004. ISBN 1-85233-694-3.

[17] A. Bemporad, F. Borrelli, and M. Morari, Piecewise linear optimal controllers for hybrid systems in Proc. Amer. Control Conf., Chicago, IL, 2000, pp. 1190–1194.

[18] A. Bemporad, M. Morari, V. Dua, and E. N. Pistikopoulos . The explicit linear quadratic regulator for constrained systems Automatica, vol. 38, no. 1, pp. 3–20, 2002.

[19] A. Bemporad, F. Borrelli, and M. Morari . Model Predictive Control Based on Linear Programming - The Explicit Solution IEEE Transactions on automatic control, VOL. 47, NO. 12, 2002

[20] F. Borrelli, M. Baoti, A. Bemporad and M. Morari . Dynamic programming for constrained optimal control of discrete-time linear hybrid systems Automatica 41 (2005) 1709–1721

[21] M. Kvasnica, P. Grieder and M. Baoti Multi-Parametric Toolbox (MPT), 2004

APPENDIX

HYSDEL CODE: Greenhouse plant
SYSTEM greenhouse {

INTERFACE {

STATE {REAL x1 [16,22];
REAL x2 [16,22];
REAL x3 [16,22];
REAL x4 [0,1]; }
INPUT { REAL u1 [0,22];
REAL u2 [0,40];
REAL u3 [0,40];
REAL u4 [0,40];
REAL u5 [0,40];
BOOL u6;}
OUTPUT {REAL y;}

PARAMETER {
REAL a11 = 1.026; REAL a21 = 0.1883; REAL a31 = -0.3575; REAL a51 = 0.0732; REAL a61 = -0.0132; REAL a71 = 0.0735; REAL a81 = -0.0003; REAL a91 = -0.0082; REAL a12 = 0.9982; REAL a22 = 0.2815; REAL a32 = -0.3757; REAL a52 = 0.0466; REAL a62 = 0.045; REAL a72 = -0.0093; REAL a82 = 0.0015; REAL a92 = 0.0019; REAL a13 = 0.8704; REAL a23 = 0.2843; REAL a33 = -0.2197; REAL a53 = 0.04315; REAL a63 = 0.0064; REAL a73 = 0.008; REAL a83 = 0.0003; REAL a93 = 0.0067; REAL a14 = 0.8189; REAL a24 = 0.3111; REAL a34 = -0.1766;REAL a54 = 0.0475; REAL a64 = -0.0114; REAL a74 = 0.0108; REAL a84 = 0.0019; REAL a94 = 0.0051; REAL a4 = 0.6; REAL T1 = 8.0001; REAL T2 = 13.0001; REAL T3 = 15.0001; REAL T4 = 17.0001;REAL T5 = 18;}}

IMPLEMENTATION {

AUX {

REAL z1,z12,z13,z14,z2,z22, z23,z24, z3, z32,z33,z34,uc,uc2,uc3,uc4,ul,zt1,zt2,zt3,uct,ult;

BOOL e1,e2,e3,e4,e5,e6,e7,e8,e9;}

AD { e1 = u1<=T1; e2 = u1<=T2; e3 = u1<=T3;e4 = u1<=T4; e5 = u1<=T5; e6 = T1<=u1;e7 = T2<=u1; e8 = T3<=u1; e9 = T4<=u1; }

DA {z1 = {IF e1 THEN a31*x1};
z12 = {IF e2&e6 THEN a32*x1}
z13 = {IF e3&e7|e5&e9 THEN a33*x1};
z14 = {IF e4&e8 THEN a34*x1};
z2 = {IF e1 THEN a21*x2};
z22 = {IF e2&e6 THEN a22*x2};
z23= {IF e3&e7|e5&e9 THEN a23*x2}
z24 = {IF e4&e8 THEN a24*x2};
z3 = {IF e1 THEN a11*x3};
z32 = {IF e2&e6 THEN a12*x3};
z33 = {IF e3&e7|e5&e9 THEN a13*x3};
z34 = {IF e4&e8 THEN a14*x3};
ul = {IF u6 THEN a4 ELSE 0};
uc = {IF e1 THEN a51*u1+a61*u2+a71*u3+ a81*u4+a91*u5};
uc2= {IF e2&e6 THEN a52*u1+a62*u2+ a72*u3 +a82*u4+a92*u5};
uc3={IFe3&e7|e5&e9THENa53*u1+a63*u2+a73*u3+a8 3*u4+a93*u5};
uc4 = {IF e4&e8 THEN a54*u1+a64*u2+ a74*u3 +a84*u4+a94*u5};}

LINEAR {zt1= z1+z12+z13+z14;
zt2= z2+z22+z23+z24;
zt3= z3+z32+z33+z34;
uct= uc+uc2+uc3+uc4;
ult= ul/a4;}

CONTINUOUS { x1=x2;
x2=x3;
x3=zt1+zt2+zt3+uct+ul;
x4=ult; }

OUTPUT {y =x3;}}}

Ibtissem Laribi Maatoug received the Engineer diploma in Electrical Engineering from the National School of Engineering in Tunis (ENIT), and prepares a PhD degree at INSAT of Tunisia. Her employment experience included the Siemens Tunisia Company, in the special fields of Industrial automation and supervision. She is currently a Researcher at the laboratory of Automatic and applied Informatics "AIA" at INSAT of Tunisia. Her research interests include Hybrid system, constrained optimal control, model predictive control, and Industrial applications of automatic control.

Radhi Mhiri received his M.Sc.and PHD degrees in automatic control from the Tunis University (ENSET), Tunisia, in and his Habilitation in electrical engineering from the Tunis El Manar university (ENIT) , Tunisia 2000. Currently, he is full professor in the Department of Physics at Tunis El Manar University, Tunisia. He is collaborator member of the Center for Research in Higher Education (CRHE) at Sherbrooke university. He is the Head of a research group (AIA) on automatic control at his university, he has published about 100 refereed journal and conference papers. His current research interests include feedback control systems, and control theory, hybrid system, elearning.

www.icgst.com

Enhancement of Voltage Stability in Radial Distribution System Using Artificial Neural Networks

V. Ganesh[1], S. Sivanagaraju[2], Ch.SaiBabu[2]
[1] *EEE Department, JNTU College of Engineering, pulivendula.Kadapa, Andhra Pradesh, India, gani_vg@yahoo.com*
[2] *EEE Department r, JNTU College of Engineering, Anantapur Andhra Pradesh, India.*
sirigiri70@yahoo.co.in
http://www.jntu.ac.in

Abstract
Network reconfiguration of distribution system is an operation in configuration management that determines the switching operations to enhance the voltage stability. Network reconfiguration for time varying loads is complex and extremely non-linear optimization problem, which can be effectively solved by artificial neural networks [ANNs], as ANNs are capable of learning a tremendous verity of pattern mapping relationships without having a priori knowledge of mathematical function. In this paper, a generalized ANN model for on-line enhancement of fast voltage stability index of radial distribution system under varying load conditions is proposed. The training sets for the ANN are carefully selected to cover the entire range of input space. The proposed ANN is trained using Levenberg-Marquardt Back Propagation algorithm and tested by applying arbitrary input data generated from Daily load curves(DLCs) for the 16 bus test system.

Keywords: *Load flows, Network reconfiguration, fast voltage stability index, Artificial neural networks*

1. Introduction
With the advent of fast computing systems, the advance control of electrical power systems has become a viable one. Owing to the fast growth in power demand of certain industrial power networks, incidence of sudden voltage collapse has been experienced. When such an incident happen from some industrial loads will be switched off through automatic cut-off switches, resulting in severe interruption. Distribution network reconfiguration can be used as a planning and a real time control tool. Most distribution networks use sectionalizing switches that are normally closed and tie switches that are normally opened. These switches are used for both protection and network reconfiguration. From time to time, modifying the radial structure of the feeders by changing the ON/OFF status of sectionalizing and tie switches to transfer loads from one feeder to another may significantly improve the operating conditions of the overall system. Feeders in distribution system normally have a mixture of industrial, commercial, residential and lighting loads. The peak load on the substation transformers and feeders occur at a different time of the day; therefore, the distribution system becomes heavily loaded at certain times of the day and lightly loaded at other times. If the distribution loads are rescheduled more efficiently by network reconfiguration, the voltage stability in the system can be improved. Reconfiguration also allows smoothening out the peak demands, improving the voltage profile in the feeders, and increasing the network reliability. Generally, network reconfiguration problems consume more time to obtain the optimal solution and difficult to online implementation, especially for big systems. Therefore, to reduce the computational burden, an intelligent based strategy may be more useful, by which an optional solution can be obtained quickly on an automated distribution system.

Literature survey shows that, lot of work has been done on the voltage stability analysis of transmission systems [1]. The voltage stability phenomenon has been well recognized in distribution systems [2]. Several analytical techniques have been proposed to assess the voltage instability. The normal operation of electrical power systems requires that the voltage magnitude be kept with in the range of about ± 5% of the nominal value. Voltage stability has been defined as ability of a system to maintain voltage at all parts of the system so that with the increase of the load, load power will increase and power and voltage are controllable [3]. Voltage stability is important for power system operation and planning because voltage instability may lead to voltage collapse, and hence outage and monetory losses, and possibly total system blackout. Artificial neural networks provide techniques for solution of some engineering problems. Their flexible nature allows Representation of many types of data for analysis. Since training is based on the

past as well as existing data of different parameters, the results obtained can be more reliable.

El-Kady et. al [4] introduced an ANN based technique for prediction of voltage stability in electrical power systems. Selection of input variables for training ANN is obtained using a performance index, which reflects the proximity of system from voltage collapse. Abd El-Aziz et. al [5] investigated the application of artificial neural networks in voltage stability assessment using the energy function method. This technique is used for calculation of voltage stability margins. El-Keib et. al [6] used the ANN's for determining the voltage stability margins based on energy function method. A systematic method for selecting the ANN's input variables was developed using sensitivity analysis. Jeyasurya [7] used the ANN's for evaluation of on-line voltage stability in modern energy control centers based on an energy measure, which is an indication of the power system's proximity to voltage collapse. Salama et. al [8] applied the ANN's to predict the voltage instability based on a voltage collapse proximity indicator, which was presented in[9].M.Chakravarthy et. al [7] has proposed voltage stability analysis of radial distribution networks.P.V Prasad et. al [16] has been proposed G.A method to solve the on-line network reconfiguration problem for enhancing the voltage stability in radial distribution system.

Artificial Neural network (ANN) is a system loosely modeled on the human brain. The main reasons are the ability of ANN to learn complex non-linear relations, and their modular structure, which allows parallel processing. Neural networks are mainly categorized by their architecture (number of layers), topology(connectivity pattern, feed forward or recurrent etc) and learning regime. One of the main features of ANN is once it is selectively trained in offline which can lead to sufficiently accurate online response.

In this paper, a generalized neural network model is proposed to solve the network reconfiguration problem for enhancing the fast voltage stability index in radial distribution systems. In the proposed model, a single neural network has been used to determine the effective switching status of dynamic switches, which enhance the voltage stability in the systems. To simplify the problems of the input data generation, the load levels of various load types P and Q obtain from the DLCs are used as inputs. The number of outputs of ANN depends on the number of dynamic switches in the network. The enhancement of fast voltage stability is obtained by using proposed ANN model by reconfiguring the network structure without any additional equipment, thus avoiding the extra installation cost involved. The effectiveness of the proposed method is tested with IEEE 16-node system

The remainder of the paper is organized as follows: Section (2) focuses on mathematical modelling of fast voltage stability index. Section (3) emphasizes on ANN training and test cases.

2. Mathematical formulation for fast voltage stability index:

Voltage stability index is an instrument to analyze the voltage stability. This index speeds up the analysis and hence called Fast Voltage Stability Index (FVSI). It can be either referred to a bus or a line but here it refers to a distribution line. For safer operation of the system it is preferred that FVSI should be less than unity. FVSI value closed to 1.00 indicates that the particular line is on the verge of instability. When the FVSI value exceeds unity it indicates that the corresponding distribution line or the bus is highly unstable and highly prone to collapse. Let us consider a two-bus system as shown in Fig 1.Consider a branch connected between busses 1 and 2 as shown in figure 1.

In figure 1, $V_1\angle\delta_1$ and $V_2\angle\delta_2$ are the voltage magnitudes and phase angles of nodes 1 and 2 respectively and the current flowing through branch is I_1. The substation voltage is assumed to be 1.0+j0.0 p.u.

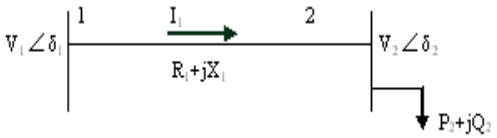

Figure.1 Electrical equivalent of a typical branch connected between two busses of a distribution system.

P_2 =Total active power load fed from node 2 including local load and total active power losses beyond node 2.
Q_2 =Total reactive power load fed from node 2 including local load and total reactive power losses beyond node 2.
From figure. 1, the line current is given by

$$I_1 = \frac{V_1\angle\delta_1 - V_2\angle\delta_2}{R_1 + jX_1} \quad (1)$$

The complex power is expressed as $S_2 = V_2.I_1^*$

$$\therefore I_1 = \{S_2 / V_2\}^* \quad (2)$$

Equating eqns.(1)and (2),we get

$$\left\{\frac{S_2}{V_2}\right\}^* = \frac{V_1\angle\delta_1 - V_2\angle\delta_2}{R_1 + jX_1} \quad (3)$$

$$\left\{\frac{P_2 - jQ_2}{V_2\angle -\delta_2}\right\} = \frac{V_1\angle\delta_1 - V_2\angle\delta_2}{R_1 + jX_1} \quad (4)$$

From eqn.(4), we get

$$\{P_2 - jQ_2\}\{R_1 + jX_1\} = V_2\angle -\delta_2\{V_1\angle\delta_1 - V_2\angle\delta_2\} \quad (5)$$

$$R_1P_2 - jR_1Q_2 + jX_1P_2 + XQ_2 = V_1V_2\angle(\delta_1 - \delta_2) - V_2^2 \quad (6)$$

$$\{R_1P_2 + X_1Q_2\} - j\{R_1Q_2 - X_1P_2\} = V_1V_2\{Cos(\delta_1 - \delta_2) + jSin(\delta_1 - \delta_2)\} - V^2{}_2 \quad (7)$$

The real part of eqn.(7) is

$$R_1P_2 + X_1Q_2 = V_1V_2Cos(\delta_1 - \delta_2) - V_2{}^2 \quad (8)$$

and imaginary parts is

$$R_1Q_2 - X_1P_2 = -V_1V_2Sin(\delta_1 - \delta_2) \quad (9)$$

or $$P_2 = \frac{V_1V_2Sin(\delta_1 - \delta_2) + R_1Q_2}{X_1} \quad (10)$$

Substituting eqn. (10) in eqn. (9) we get

$$V_1V_2Cos(\delta_1 - \delta_2) - V_2{}^2$$

$$V_2{}^2 + V_1V_2\left\{\left(\frac{R_1}{X_1}\right)Sin(\delta_1 - \delta_2) - Cos(\delta_1 - \delta_2)\right\} + Q_2\left\{\left(\frac{R_1{}^2}{X_1}\right) + X_1\right\} = 0$$

(11)

This quadratic equation when solved gives the solution for V_2

$$V_2 = \frac{\left\{-V_1\left\{\left(\frac{R_1}{X_1}\right)Sin(\delta_1-\delta_2)-Cos(\delta_1-\delta_2)\right\}\right\} \pm \sqrt{\left\{\left\{\left(\frac{R_1}{X_1}\right)Sin(\delta_1-\delta_2)+Cos(\delta_1-\delta_2)\right\}^2 V_1^2\right\} - 4\left(\frac{Q_2}{X_1}\right)\left\{R_1^2+X_1^2\right\}}}{2}$$

(12)

To obtain the real roots of V_2 the discriminate has to be sent to zero or positive

$$\therefore V_1^2\left\{\left(\left(\frac{R_1}{X_1}\right)(Sin(\delta_1-\delta_2)+Cos(\delta_1-\delta_2)\right\}^2 - 4\left(\frac{Q_2}{X_1}\left\{R_1^2+X_1^2\right\}\right) \geq 0$$

$$V_1^2\left\{\left(\left(\frac{R_1}{X_1}\right)\right)Sin(\delta_1-\delta_2)+Cos(\delta_1-\delta_2)\right\}^2 - 4\left(\frac{Q_2}{X_1}\right)Z_1^2 \geq 0$$

$$V_1^2\left\{\left(\left(\frac{R_1}{X_1}\right)Sin(\delta_1-\delta_2)Cos(\delta_1-\delta_2)\right\}^2 \geq 4Z_1^2\left(\frac{Q_2}{X_1}\right)\right.$$

$$FVSI = \frac{4Z_1^2 Q_2}{V_1^2 X_1\left\{\left(\left(\frac{R_1}{X_1}\right)\right)Sin(\delta_1-\delta_2)+Cos(\delta_1-\delta_2)\right\}^2} \leq 1$$

In generalized for $\mathbf{FVSI_{(i)}}$ is =

$$\frac{4Z_j^2 Q_{i+1}}{V_i^2 X_j\left\{\left(\left(\frac{R_j}{X_j}\right)\right)Sin(\delta_i-\delta_{i+1})+Cos(\delta_i-\delta_{i+1})\right\}^2} \leq 1 \qquad (13)$$

…

3. Development of ANN model for enhancement of voltage stability through Network reconfiguration

The ANN based techniques map the nonlinear relationship between the load patterns and the corresponding optimal system topologies and determine the most appropriate system topology according to the current load pattern on the basis of the trained knowledge. The relationship between load patterns and the corresponding switching states in the network is mapped into an ANN by training it using back propagation algorithm. From the observation in network reconfiguration for enhancing fast voltage stability, it is found that only a few switches change their ON/OFF states from time to time to achieve optimal network configuration. For solving the fast voltage stability problem, a single ANN model is developed to determine the status of all the dynamic switches in the network. By considering the load variations on the load curves of different load types, the input training sets for the ANN are generated. The output of the ANN is the switch-status of the dynamic switches obtained from the off-line simulation using analytical procedure [14].

3.1 Training –data generation for ANN model

The loads of the network can be classified into residential, commercial and industrial, lighting and other types of load groups. The load characteristics of each group are similar, and their load duration curves are also unique. Also, it is to be noted that the changes of loads in each load group show a similar trend. The daily load curves show the consumers demand at different times of the day. By observing the trend of daily load curves, the distribution networks can be operated optimally to keep the voltage stability at a maximum, and neural network model can be implemented to take care of optimal operation of the distribution network at all times. To generate the input vectors for the ANN model form the load curves, the percentage of peak load at every time instance is considered. The input vectors at every regular interval of time are generated by obtaining the percentages of peak demand from the DLCs. Normally, DLC represents the real and reactive load demands at different times of the day.

The network in any automated distribution system is reconfigured from time to time to enhance the fast voltage stability at all times by changing the ON/OFF status of the sectionalizing and tie switches. The switching states of optimal configuration for voltage stability are determined beforehand by off-line simulation using a standard algorithm for fast voltage stability enhancement. The switching for each input vector of the training set is found by simulation. From the simulation results it is found that many of the switches do not change their status, which can be named as static switches. To achieve the optimal configuration for fast voltage stability enhancement, only few switches are found to change their states, and these switches are named as dynamic switches. Therefore, the ON/OFF states of the dynamic switches are considered as the outputs of the ANN model. The number of dynamic switches in the system is represented by the number of output neurons in the ANN model.

3.2 Design of ANN model

The network reconfiguration problem has an extremely non-linear relationship between input loads and the status of dynamic switches. Hence, back propagation neural network is most suitable for network reconfiguration problem. Figure 2 shows the ANN architecture used for designing the ANN model for the prediction of switching status of dynamic switches in the network reconfiguration scheme employed in this paper.

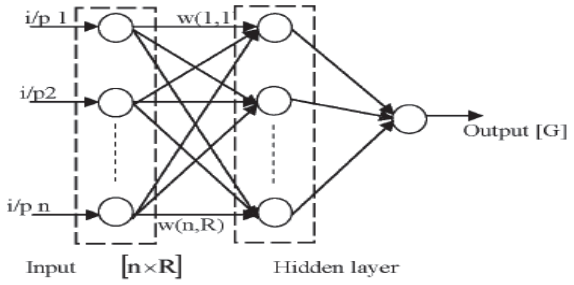

Figure. 2. Architecture of ANN model

3.3 ANN Assessment of fast voltage stability index

A multi layer feed forward artificial neural network with back propagation learning is proposed for the prediction of the fast voltage stability index. This reflects the

proximity of the distribution system to voltage collapse. The ANN based technique maps the relationship between the load total active and reactive powers of the distribution system and the fast voltage stability index according to the present loading pattern. The fast voltage stability index is obtained on each bus by using certain reconfiguration of the distribution system. Therefore it is a model for the network reconfiguration by a certain neural network pattern. This technique helps to study the effect of the load at each bus on by enhancing the fast voltage stability index.

3.4 On- Line implementation of ANN model

To enhance the fast voltage stability, the variations are to be monitored continuously by selecting appropriate switching status of the switches (Dynamic switches, tie switches etc.) in loads profile. Network reconfiguration is done time to time according to the load scheduling to obtain maximum voltage stability. The developed ANN model can be implemented effectively in real time control of on-line systems. Using load-monitoring packages such as DAS (Distribution automation system) and SCADA, the data from the remote units of the distribution network are gathered and applied to the ANN model. The ANN model can be used to determine the optimal switching configuration and a decision made by the control system strategy by sending the appropriate control signal to the controller. The controller, in turn, is used to activate the proper switches to implement the optimal switching configuration for enhancing fast voltage stability.

3.5 Test system

To demonstrate the potential value of the developed ANN model, IEEE 16-node distribution system with 13 sectionalizing switches and 3 tie switches is considered as a test case as shown in figure 3**.** The peak load, line and tie switch data are given in Appendix**.** For simplicity, it is assumed that there are only three types of loads residential, commercial and industrial and are indicated in the table. A given in Appendix. It is also assumed that the load of each node varies independently.

4.Test of ANN model

The components of each input vector are the actual loads (P_i, Qi) in terms of percentages of peak demand found from the daily load curves. The output for each input vector is the switching options computed through off-line simulation of branch exchange algorithm for voltage stability [12]. DLCs for residential, commercial and industrial type of loads for a weekday are shown in fig. 5 . The percentages of peak demand are obtained at every 10-minute time interval, and hence the total time period T (24 hours) is divided into 144 equal time intervals. As there are only three types of loads considered in this example, the input matrix will be [6 ×144] for each input vector the output for the ANN is determined by actual off- line simulation. From the simulation results, it is found that only three switches (④, ⑧, ⑪) change their ON/OFF status. Therefore, these three switches are considered as the dynamic switches. Table 1 shows the grouping of the switches, in which there are 10 static switches, 3 dynamic switches and 3 tie switches.

As the three switches only change their status and others remain unchanged at all times, the ON /OFF status of these three switches will be the output of the ANN model. The number of output neurons of the ANN will be three and each output either 1 or 0. The ANN model is constructed using 6 input and 3 output neurons. The ANN model is trained vectors employing the Levenberg-Marquardt algorithm . The test results are found to coincide with the actual outputs obtained from simulation results for the test input vectors given in table 2.

The DLC of a Week day is represented in figure 4 where figure4(a) represents the Residential load curve in percentage of peak load. Figure4(b) represents the Commercial load curve in percentage of peak load and figure4(c) represents the Industrial load curve in percentage of peak load

5.Conclusion

A generalized ANN model has been proposed in this paper to reconfigure the network for enhancing the fast voltage stability index of radial distribution systems. The actual loads in terms of percentages of peak demand obtained from DLCs of different types of loads at specified time intervals are generated for training the ANN model. To show the performance of the proposed ANN model, a 16-node test system is used and the model is trained by applying the input vectors generated for the system using Lavenberg-Marquardt Back propagation algorithm. The accuracy of the ANN results indicates that the ANN model can be a useful tool for solving on-line real time network reconfiguration problems of the distribution system. From the results it is observed that the fast voltage stability index has improved due to improvement of minimum voltage level shown in figures 5 and 6. Table 2 shows the test results obtained from the ANN model and the simulation are nearly equal.

Table 1

Switch-groups in terms of their operating conditions

Types of switches	Switches
Static switches	①,②,③,⑤,⑥,⑦,⑨,⑩,⑫,⑬
Dynamic switches or (Sensitive switches)	④, ⑧, ⑪
Tie switches	⑭, ⑮, ⑯

Table 2

Test results obtained from ANN model and simulation

Input-sets for testing						Actual output simulation			Outputs of ANN model		
Res(%)		Com(%)		Ind(%)							
P	Q	P	Q	P	Q	④	⑧	⑪	④	⑧	⑪
45	40	29	45	46	35	2.99×10^{-5}	3.31×10^{-6}	1.15×10^{-5}	0	0	0
49	42	32	46	48	37	1.04×10^{-5}	4.65×10^{-6}	4.41×10^{-7}	0	0	0
55	42	40	51	60	46	4.29×10^{-4}	3.54×10^{-6}	2.62×10^{-5}	0	0	0
60	45	85	76	90	71	1	1.28×10^{-6}	0	1	0	0
65	43	88	76	93	68	1	0	4.66×10^{-6}	1	0	0
70	37	79	70	88	60	1	0	2.87×10^{-5}	1	0	0
80	44	69	64	70	46	0	0	0.00117	0	0	0
85	47	72	62	68	44	0	0	0.1235	0	0	0
90	49	71	63	59	40	0.8878	0	1	1	0	1
100	49	59	60	43	33	0	6.13×10^{-6}	1	0	0	1
80	45	45	50	43	31	3.01×10^{-5}	0	1	0	0	1
60	42	41	48	44	32	4.73×10^{-5}	0	5.72×10^{-4}	0	0	0


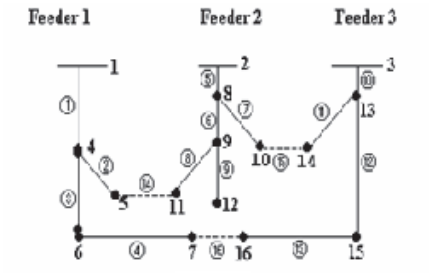

1,2,3,….,nodes. ①,② ...,switch numbers

Figure 3. Schematic diagram of 16-node test system

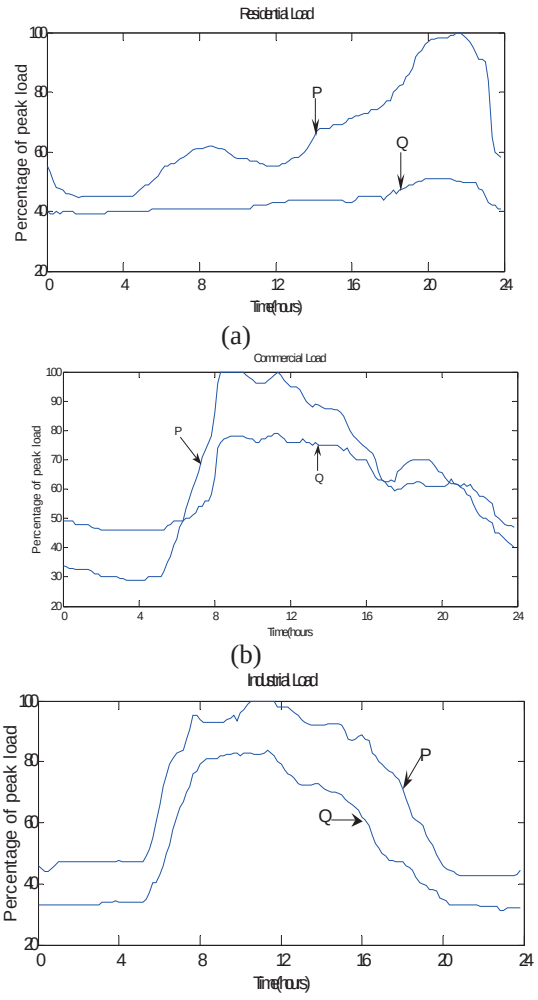

Figure 4.: (a) Residential load curve in percentage of peak load (b) Commercial load curve in percentage of peak load and (c) Industrial load curve in percentage of peak load

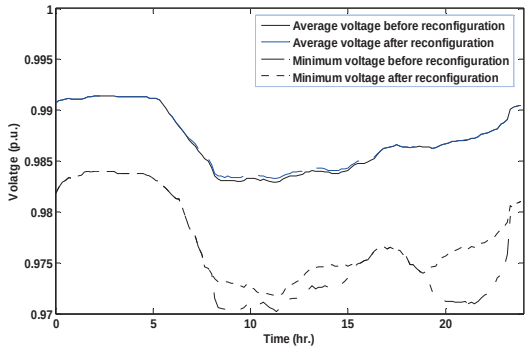

Figure 5 . Average voltage and minimum voltage(p.u) w.r.t to Time

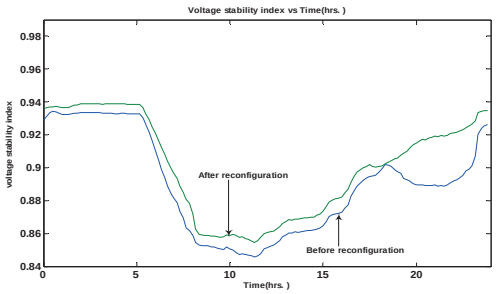

Figure 6 Fast Voltage stability index w.r.t to Time

6. References

[1] V.Ajjarapu and B.Lee, "Bibliography on voltage stability," IEEE Transactions on Power Systems, Vol.13, No.1, pp. 115-125, February 1998.

[2] F.Gubina and B.Strmcnic, " A Simple approach to voltage stability assessment in radial distribution networks , " IEEE Transactions on Power Systems, Vol. 12, No. 3, pp.1121-1128, August 1997.

[3] IEEE Publications 90th 0358-2-PWRS, "Voltage stability of power system : concepts, analytical tools and industry experience," IEEE Service center, Piscataway New Jersey 1990.

[4] F. M. El-Kady and A.Y. Abd El-Aziz, "Voltage Stability Assessment of Electrical Power System Using Artificial Neural Networks," Journal of Engineering and Applied Science, Vol. 48, No. 4, PP727-743, August 2001.

[5] A. El-Keib and X. Ma, "Application of artificial neural networks in voltage stability assessment," IEEE, Trans. On Power Systems, vol.10, no. 4, pp. 1890-1896, November 1995.

[6] M. M. Hamada, M. A. A. Wahab and N. G. Hemdan, "A references new Criterion for Assessing Voltage Stability in radial Distribution Systems," Proc. MEPCON, Tenth International Middle East Power System conference, Portsaid, Egypt, Vol. Vol. 23, PP. 129-135, 2001.

[7] M. Charkravorty and D. Das, "Voltage Stability Analysis of Radial Distribution Networks," Electrical Power & Energy no. 2, Vol . 23, PP. 129-135, 2001.

[8] M. J.H. Sterling, M.Chebbo, and M.R Irving, "Reactive power dispatch incorporating voltage stability," IEE Proc- C, Vol. 139, No. 3, pp. 253-260, 1992.

[9] G. B. Jasmon and L.H.C.C.Lee, "Maximizing voltage stability in distribution networks via loss minimization," Electrical Power and Energy Systems, Vol. 13, No. 3, pp. 148-152, 1991.

[10] A. Sallam, M. E. Aboul-Ela and E. E. Elaraby, "Monitoring and control of voltage stability in power systems," Proceedings of EMPD-95, Singapore, November 21-23, pp. 342-347, 1995.

[11] K.Pal, "Voltage stability conditions considering load characteristics," IEEE Transactions on Power Systems, Vol. 7, No.1, pp. 243-249, 1992.

[12] R.Laches and D.Sunato, "Different types of voltage instability," IEEE Trans. On Power Systems,Vol. 9, No.2, pp.1126-1134, 1994.

[13] T.S. Dillon, "Artificial Neural Network applications to symbolic methods," Electrical Power and Energy Systems, Vol. 13, No. 2, pp. 66-72, 1991.

[14] M.A Kashem, G.B. Jasmon , A..Mohamed, and M. Moghavvemi, "Artificial neural Network approach to network reconfiguration for loss minimization in Distribution Networks". Electrical Power and Energy Systems, Vol. 20, No. 4, pp. 247- 258, 1998.

[15] S.Sivanagaraju, et. al, " Enhancing voltage stability of radial distributions by network reconfiguration," Electric Power Components and Systems, Vol. 33, pp. 539-550, 2005.

[16]. P.V Prasad, S.Sivanagaraju , N.Srinivasulu "Enhancement of voltage stability in radial distribution systems using Genetic Algorithm" Water and energy international journal , vol 64, N0. 3, sept 2007, pp 29 – 35.

Appendix A: Peak demand load data of the 16-node test system

Line		Impedance		Receiving node load (Peak demand)		
Sending node	Receiving node	R (p.u)	X(p.u)	MW	MVAR	Load type
1	4	0.15821	0.30395	2.10	0.92	R
4	5	0.09487	0.18237	1.75	0.87	R
4	6	0.27323	0.52522	1.25	0.65	R
6	7	0.31624	0.60790	1.10	0.52	C
2	8	0.13282	0.25532	1.28	0.76	C
8	9	0.12650	0.24316	1.65	0.78	C
8	10	0.12396	0.23830	1.30	0.78	C
9	11	0.09993	0.19210	0.94	0.56	I
9	12	0.26564	0.51064	1.45	0.59	R
3	13	0.18974	0.36474	1.42	0.68	C
13	14	0.12396	0.23830	1.98	0.79	I
13	15	0.11258	0.21641	1.45	0.67	I
15	16	0.18974	0.36474	1.08	0.45	I
5	11	0.14926	0.28693	---	---	---
10	14	0.19986	0.38419	---	---	---
7	16	0.15812	0.30395	---	---	---

* R: Residential; C: Commercial; I: Industrial

Where

V_i is the voltage at node i

R_j is the resistance of branch j

X_j is the reactance of branch j

δ_i, δ_{i+1} is the phase angles at node i and i+1

Z_j is the impedance of branch j

Q_{i+1} is the reactive power at node i+1.

Bibliographies

V.Ganesh, is graduated in 1998, Masters in 2004 from S.V.University, Tirupathi and currently pursuing his Ph.D from J.N.T.University, Hyderabad, india. He is Working as Assistant Professor in the Department of Electrical Engineering, J.N.T.University, pulivendula, Kadapa, Andhra Pradesh, india .
His areas of interest are Neural Networks and its applications in Electrical Distribution systems and Distribution automation.

Dr.S.Sivanagaraju, is graduated in 1998, Masters in 2000 from IIT, Kharagpur and did his Ph.D from J.N.T.University in 2004. Working as Associate Professor in the Department of Electrical Engineering, J.N.T.U College of Engg. (Autonomous), Anantapur, Andhra Pradesh , india. He has received two National awards (Pandit Madan Mohan Malaviya memorial prize award and Best Paper Prize award) from the Institute of Engineers (India) for the year 2003-2004. He is Referee for IEE Proceedings- Generation Transmission and Distribution and International Journal of Emerging Electric Power System. About 40 publications in National and International Journals and Conferences to his credit.
His areas of interest are in Distribution Automation, Genetic Algorithm applications to distribution systems and power system.

Dr.Ch.SaiBabu did his Ph.D from J.N.T University. Working as Professor in the Department of Electrical Engineering, J.N.T University. Anantapur, Andhra Pradesh. India.. He has 20 publications in National and International Journals and Conferences to his credit. His areas of interest are in Power system reliability , fuzzy and ANN applications to different areas in electrical engineering.

www.icgst.com

A NOTE ON PROCEDURES FOR CHECKING PERSISTENCY OF EXCITATION

W. C. Leite Filho
Senior Researcher - Space and Aeronautics Institute
12228-904, São José dos Campos, Brazil
waldemar@iae.cta.br

Abstract

This work describes a sufficient condition for a quasi-stationary deterministic *m*-vector signal to be persistently exciting of order *n*, using the spectral density matrix estimate based on the Finite Fourier Transform FFT. It is shown that the spectral density matrix of any periodic noise-free vector signal has rank one. Moreover, it is shown that the usual assumption that the spectral density matrix should be positive definite is not applicable in this case. A procedure for checking the order of persistence is presented.

Keywords*: persistent excitation, spectral density matrix, persistence checking*

1. Introduction

The concept of persistent excitation (PE) plays an important role in the convergence of parameters of adaptive controllers [1-3] and in the convergence of parameters in identified models [4, 5]. In qualitative terms it expresses the notion that the input signal to the plant should be such that all the modes of the plant are excited if perfect identification is to be achieved.

Several equivalent definitions exist for PE in terms of the frequency content of the input signal [2, 4, 5], non-singularity of a covariance matrix [6], and linear independence of the values of a time-varying vector over an interval [1-3, 7].

It is important to notice the difference between persistency level and persistency order [2]. Level of persistency regards time domain, while order of persistency refers to frequency domain. Besides the PE order *n* can be smaller or even bigger than the order *m* of ***u****(t)*.

In this paper the frequency domain approach will be considered, since the order of persistency is fundamental information to the identification processes [4, 5].

When ***u****(t)* is a *m*-vector, it implies that its spectral density matrix $\mathbf{\Phi_u}(\omega)$ is an $m \times m$ matrix. To check if ***u****(t)* is persistently exciting it is usual to assume that $\mathbf{\Phi_u}(\omega)$ is positive definite for at least *n* distinct frequencies [4]. However, this work aims to show that when deterministic signals are being dealt with and one estimates $\hat{\mathbf{\Phi}}_u(\omega)$ using a FFT-based spectral estimator, the rank of $\hat{\mathbf{\Phi}}_u(\omega)$ is found to be 1.

This raises the question: if $\hat{\mathbf{\Phi}}_u(\omega)$ cannot be positive definite for $n \geq 2$, how can one check whether or not a *m*-vector is PE of order n, by using an FFT-based spectral density matrix estimator? This work proposes an alternative procedure for checking the order of persistence.

The paper is organized as follows: Section (2) focuses on the definition of persistent excitation and on the problem formulation. Sections (3 & 4) describe the development of the algorithm proposed for checking the order of persistent excitation. Section (5) gives an example of the algorithm application. Section (6) provides the conclusion. Section (7) lists the references used in the paper.

2. Problem Description

The frequency domain definition of persistent excitation [5] is the following:

A quasi-stationary signal $\{u(t)\}$, with spectral density matrix $\Phi_u(\omega)$, is said to be persistently exciting of order *n* if, for all filters of the form

$$M_n(q) = m_1 q^{-1} + ... + m_n q^{-n} \tag{1}$$

where q^{-1} is the backward shift operator, the relation

$$\left| M_n(e^{j\omega}) \right|^2 \Phi_u(\omega) \equiv 0 \tag{2}$$

implies that $M_n(e^{j\omega}) \equiv 0$.

As a direct consequence of the definition, *u(t)* is PE of order *n*, if $\Phi_u(\omega)$ is different from zero in, at least, n points in the interval $-\pi < \omega \leq \pi$.

Persistence of excitation of an m-dimensional signal $\{\mathbf{u}(t)\}$ is defined analogously:

In this case, as before,

$$\mathbf{M}_n(q) = \mathbf{m}_1 q^{-1} + ... + \mathbf{m}_n q^{-n} \tag{3}$$

with $\mathbf{m}_{i\,;\,i=1,..,n}$ as m × m matrices. Then ***u****(t)* is said to be PE of order *n* if the equation

$$\mathbf{M_n}(e^{j\omega})\mathbf{\Phi_u}(\omega)\mathbf{M_n^T}(e^{-j\omega}) \equiv 0 \quad (4)$$

implies that $\mathbf{M_n}(e^{j\omega}) \equiv 0$.

It is important to notice that the order *n* of PE can be smaller or even larger than the dimension *m* of ***u(t)***.

When ***u(t)*** is scalar, it is easy to understand that it is sufficient to have $\Phi_u(\omega) \neq 0$ in, at least, *n* frequencies, because this raises *n* different equations $\left|M_n(e^{j\omega})\right|^2 \Phi_u(\omega) = 0$, which implies $M_n(e^{j\omega}) = 0$ and all $m_i = 0$.

Nevertheless, when ***u(t)*** is a *m*-vector, it implies that $\mathbf{\Phi}_u(\omega)$ is a matrix of dimension *m* x *m*. In a similar way, it is sufficient to assume that $\mathbf{\Phi}_u(\omega)$ is positive definite for at least *n* distinct frequencies [4]. However, the FFT-based estimate of $\mathbf{\Phi}_u(\omega)$ for deterministic signals always has rank 1.

In order to clarify this, consider a *m*-vector **u***(t)*, where each *i*-th element is composed of a sum of sinusoids, expressed by complex-valued variables

$$\mathbf{u}(t) = \sum_k \mathbf{a}_k e^{j\omega_k t}. \quad (5)$$

Then it is straightforward to derive

$$\mathbf{\Phi}_u(\omega) = \sum_k \mathbf{a}_k \mathbf{a}_k^* . \delta(\omega \pm \omega_k), \quad (6)$$

which obviously has rank 1. Therefore, this could lead to an incorrect conclusion that such a signal is not persistently exciting, even though an equation of the form of (5) represents a well-known type of PE signal (as defined in the time domain [1, 2]). In other words, this example shows that is very likely to have a PE vector signal whose spectral density matrix $\Phi_u(\omega)$ has rank 1.

The same problem can happen when we consider estimation of the spectral density matrix based on the FFT of the original data records. For a finite time interval $0 \le t \le T$ and *N* samples, define [8, 9]

$$S_{u_i u_j}(\omega, T) = \frac{1}{T} U_i^*(\omega, T) U_j(\omega, T) \quad (7)$$

where the quantity

$$U_i(\omega_k, T) = T.\sum_{l=0}^{N-1} u_i(l).\exp(-j.\frac{2.\pi.k.l}{N}) \qquad k=0,1,2,\ldots,N-1$$

represents the FFT of $u_i(l)$. This finite Fourier transform will exist in general for stationary records, whereas the equivalent infinite-range Fourier transform would not exist, since the stationary data would theoretically persist forever.

When the estimate of the spectral density matrix associated to sample records is considered over a finite time interval T, it can be computed as follows [8, 9]

$$\hat{\mathbf{\Phi}}_\mathbf{u}(\omega_k) = \begin{bmatrix} S_{u_1u_1} & S_{u_1u_2} & \cdots & S_{u_1u_m} \\ S_{u_2u_1} & S_{u_2u_2} & \vdots & \vdots \\ \vdots & \cdots & \ddots & \vdots \\ S_{u_mu_1} & \cdots & \vdots & S_{u_mu_m} \end{bmatrix} \quad (8)$$

Applied to signal (5), the spectral density matrix estimator based on FFT [8, 9], for any *k* is:

$$\hat{\mathbf{\Phi}}_\mathbf{u}(\omega_k) = \frac{\pi^2}{T} \mathbf{a}_k \mathbf{a}_k^* . \delta(\omega \pm \omega_k) \quad (9)$$

which is essentially the same result of (6).

Next, one can analyse the equation (4) and easily derive

$$\sum_k M(\omega_k)\mathbf{a}_k \mathbf{a}_k^* M^*(\omega_k) = 0 \quad (10)$$

and yet $M(\omega_k)\mathbf{a}_k = 0 \quad \forall k \quad (11)$

This may be rewritten as

$$(M_1 e^{j\omega_k} + M_2 e^{2j\omega_k} + \ldots + M_n e^{nj\omega_k})\mathbf{a}_k = 0 \quad k = 1,\ldots K \quad (12)$$

It is possible to convert (12) to a linear system of equations with respect to unknown coefficients $M_1,\ldots M_n$. Further, the explicit condition on the vector amplitudes as well as on the frequencies (12) implies that $M_1 = M_2 = \ldots = M_n = 0$.

This shows that for any periodic signal, although the spectral density matrix is not positive definite (has rank 1), it can be PE as shown according to the definition [5]. It is an important result because several frequency domain identification techniques use periodic noise-free input signals [6, 10-12].

Although this result applies to a periodic continuous signal it can be used more broadly, because the discrete-time Fourier transform of an aperiodic signal is always periodic [13]. A finite-range Fourier transform can actually be computed with digitized data, and this finite range can always be considered as the period of an associated Fourier series [9]. If we consider equation (5) for N terms and $\omega_k = 2.\pi.k/N$, it is equivalent [14] to the inverse of the Finite Fourier Transform of the truncated time signal $u_i(t), t \in [0, T]$ sampled for N points. Hence, **u***(t)* can be any quasi-stationary signal.

3. Proposed Strategy

To answer the question on how to check if a signal is PE by using the spectral density matrix, a strategy that can generalize the result of the previous section is proposed. At first, consider some properties of $\mathbf{\Phi_u}(\omega)$. It is a Hermitian matrix [15][16] and its eigenvalues are real positive quantities with orthogonal eigenvectors. Then, $\mathbf{\Phi_u}(\omega)$ can be always written in diagonal form [15], as

$$\mathbf{\Phi_u}(\omega) = \mathbf{V.D.V^T} \quad (13)$$

where $\mathbf{D} = diag\{\mu_j; j = 1,\ldots,m\}$ and

$\mathbf{V} = [V1 \quad V2 \quad \cdots \quad Vm]$ is the eigenvector matrix.

Based on the definition of PE above mentioned, the following result can be stated:

Theorem

Given a *m*-vector signal ***u(t)*** – as defined in equation (5) – now define an *mn*-vector ***W(jω)***

$$\mathbf{W}(j\omega) = \left[\vartheta_1.(j\omega)^{-1} \quad \cdots \quad \vartheta_1.(j\omega)^{-n} \quad \cdots \quad \vartheta_m.(j\omega)^{-1} \quad \cdots \quad \vartheta_m.(j\omega)^{-n} \right] \quad (14)$$

where ϑ_i, *i=1…m* are the eigenvector elements of $\mathbf{\Phi_u}(\omega)$ for all non-zero eigenvalues. If there are *mn* different

values of ω (including -ω) which leads to LI vectors $\boldsymbol{W(j\omega)}$, then $\boldsymbol{u(t)}$ is PE of order *n*.

Proof

The substitution of the equation (13) in equation (4) gives the PE definition as

$$\left[\mathbf{M_n}(e^{j\omega})\mathbf{V}(\omega)\right]\mathbf{D}(\omega)\left[\mathbf{V^T}(\omega)\mathbf{M_n^T}(e^{-j\omega})\right]\equiv 0 \quad (15)$$

where

$$\mathbf{M_n}(e^{j\omega})=\begin{bmatrix}\sum_{k=1}^{n} m_{k_{11}}(j\omega)^{-k} & \cdots & \sum_{k=1}^{n} m_{k_{1m}}(j\omega)^{-k}\\ \vdots & \ddots & \vdots \\ \sum_{k=1}^{n} m_{k_{m1}}(j\omega)^{-k} & \cdots & \sum_{k=1}^{n} m_{k_{mm}}(j\omega)^{-k}\end{bmatrix}. \quad (16)$$

Considering the spectral density matrix $\mathbf{\Phi_u}(\omega)$ for any ω_k as shown in equation (9), its corresponding diagonal matrix has only one non-null eigenvalue, since it has rank 1.

Thus, without loss of generality:

$$\mathbf{D}_{mxm}=\begin{bmatrix}\lambda & 0 & \cdots & 0\\ 0 & 0 & \cdots & 0\\ \vdots & & \ddots & \vdots\\ 0 & 0 & \cdots & 0\end{bmatrix} \quad (17)$$

and its corresponding eigenvector

$$V1=\begin{bmatrix}\vartheta_1 & \vartheta_2 & \ldots \vartheta_m\end{bmatrix} \quad (18)$$

Then, the equation (15) results in appendix equation (19)

From appendix equation (19) it's shown that all elements of the main diagonal are null. So there are *m* equations

$$\sum_{i=1}^{m}\vartheta_i\sum_{k=1}^{n} m_{k_{\ell i}}(j\omega)^{-k}=0\Rightarrow$$

$$\begin{bmatrix}\vartheta_1 & \vartheta_2 & \cdots & \vartheta_m\end{bmatrix}\begin{bmatrix}m_{1_{\ell 1}} & \cdots & m_{n_{\ell 1}}\\ m_{1_{\ell 2}} & \cdots & m_{n_{\ell 2}}\\ \vdots & & \vdots\\ m_{1_{\ell m}} & \cdots & m_{n_{\ell m}}\end{bmatrix}\begin{bmatrix}(j\omega)^{-1}\\ (j\omega)^{-2}\\ \\ (j\omega)^{-n}\end{bmatrix}=0 \quad (20)$$

where $\ell = 1\ldots m$.

Equation (20) is also equivalent to

$$\begin{bmatrix}\vartheta_1.(j\omega)^{-1} & \cdots & \vartheta_1.(j\omega)^{-n} & \cdots & \vartheta_m.(j\omega)^{-1} & \cdots & \vartheta_m.(j\omega)^{-n}\end{bmatrix}\begin{bmatrix}m_{1_{\ell 1}}\\ \vdots\\ m_{n_{\ell 1}}\\ \vdots\\ m_{1_{\ell m}}\\ \vdots\\ m_{n_{\ell m}}\end{bmatrix}=$$

$$W(j\omega)\begin{bmatrix}m_{1_{\ell 1}}\\ \vdots\\ m_{n_{\ell 1}}\\ \vdots\\ m_{1_{\ell m}}\\ \vdots\\ m_{n_{\ell m}}\end{bmatrix}=0 \qquad \ell = 1\ldots m \quad (21)$$

Considering that there are *mn* values of ω (-ω included) for $\boldsymbol{W(j\omega)}$, for each $\ell = 1\ldots m$, the matrix $\mathbf{H(}\boldsymbol{W(j\omega)}\mathbf{)}$ can be assembled as follows

$$\mathbf{H}=\begin{bmatrix}\vartheta 1_1.(j\omega_1)^{-1} & \cdots & \vartheta 1_1.(j\omega_1)^{-n} & \cdots & \vartheta 1_m.(j\omega_1)^{-1} & \cdots & \vartheta 1_m.(j\omega_1)^{-n}\\ \vartheta 2_1.(j\omega_2)^{-1} & \cdots & \vartheta 2_1.(j\omega_2)^{-n} & \cdots & \vartheta 2_m.(j\omega_2)^{-1} & \cdots & \vartheta 2_m.(j\omega_2)^{-n}\\ \vdots & & \vdots & & \vdots & & \vdots\\ \vartheta mn_1.(j\omega_{mn})^{-1} & & \vartheta mn_1.(j\omega_{mn})^{-n} & & \vartheta mn_m.(j\omega_{mn})^{-1} & & \vartheta mn_m.(j\omega_{mn})^{-n}\end{bmatrix} \quad (22)$$

$$\mathbf{H}\begin{bmatrix}m_{1_{\ell 1}}\\ \vdots\\ m_{n_{\ell 1}}\\ \vdots\\ m_{1_{\ell m}}\\ \vdots\\ m_{n_{\ell m}}\end{bmatrix}=0 \quad (23)$$

If this set of vectors is LI, then the resultant matrix **H** is invertible and the equation (23) admits only the trivial solution

$$\begin{bmatrix}m_{1_{\ell 1}} & \cdots & m_{n_{\ell 1}} & \cdots & m_{1_{\ell m}} & \cdots & m_{n_{\ell m}}\end{bmatrix}^T=0,\ \ell = 1, 2\ldots m.$$

Thus, all $m_{k_{ij}}=0$ (*i, j= 1…m* and *k =1…n*), in other words $\mathbf{M_n}(e^{j\omega})\equiv 0$. Therefore, $\boldsymbol{u(t)}$ is persistently exciting as defined previously (4). *q.e.d.*

This result implies that it's sufficient to have, at least, the nearest integer of $nm/2+1$ different frequencies (because ω and -ω are taken into account) in $\boldsymbol{u(t)}$ such that concatenation of corresponding $\boldsymbol{W(j\omega)}$ can produce a matrix **H** which has rank *mn*.

4. Checking Algorithm

The steps to check if a given *m*-vector deterministically sampled $\boldsymbol{u}$[k], k=1, 2 … N (where $T = N.\Delta t$) is PE of order *n*, are the following:

Step 1: Compute FFT of each i-th component of $\boldsymbol{u}$[k] - $U_i(\omega_k)$ and choose *mn* existing frequencies in its components (including -ω_k).

Step 2: Compute the estimate of the spectral density matrix $\mathbf{\Phi_u}(\omega_k)$ – equations (7) and (8).

Step 3: Compute the eigenvector of $\mathbf{\Phi_u}(\omega_k)$ { $\boldsymbol{V(\omega_k)}$ }- corresponding to its non-null eigenvalue.

Step 4: Based on $\boldsymbol{V(\omega_k)}$ obtained, compute the *mn*-vectors $\boldsymbol{W(\omega_k)}$ - expression (14) - for each ω_k and -ω_k chosen in step 1.

Step 5: Compute the determinant of matrix $\mathbf{H}_{mn\ x\ mn}$ composed by all *mn* vectors $\boldsymbol{W(\omega_k)}$ obtained in step 4. If the determinant is non-null, then $\mathbf{H}_{mn\ x\ mn}$ is invertible and the solution of (23) leads to the conclusion that $\boldsymbol{u}$ is PE. Otherwise, go back to step 1, choose other frequencies and try again.

The flowchart of the checking algorithm is shown below

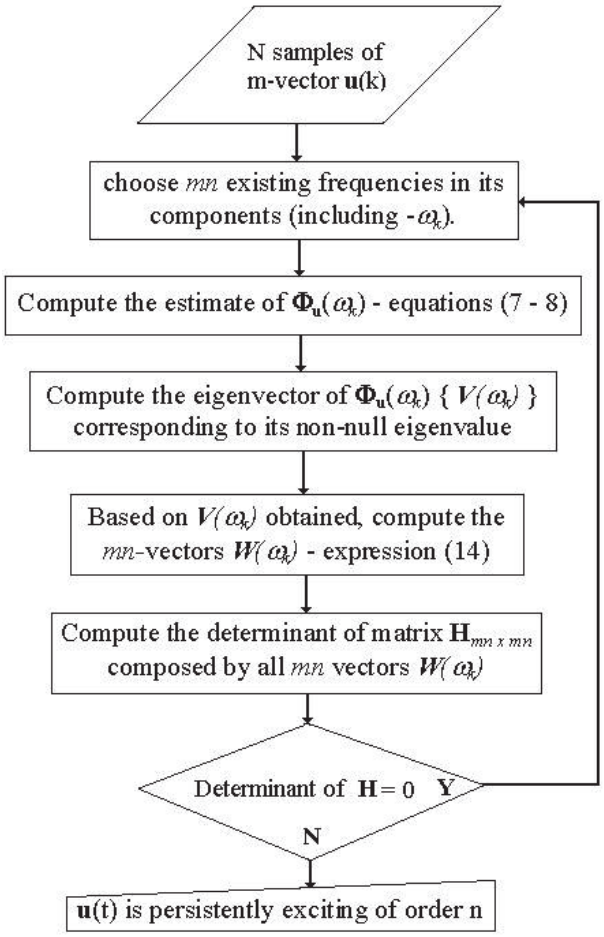

5. A Case of Study

Consider the vector $\mathbf{u}(t) = [u_1 \quad u_2 \quad u_3]^T$ where its components and the respective FFT absolute values are shown in the figures 1, 2 and 3.

Figure 4 shows the absolute values of the spectral density matrix components.

The first four frequencies are selected in order to find the following eigenvectors:

$$f = .9765\,mHz \rightarrow V1 = \begin{bmatrix} -0.0358 - 0.3952i \\ 0.7123 - 0.1541i \\ 0.5581 \end{bmatrix}$$

$$f = -.9765\,\text{mHz} \rightarrow V2 = \begin{bmatrix} -0.0358 + 0.3952i \\ 0.7123 + 0.1541i \\ 0.5581 \end{bmatrix}$$

$$f = 1.953\,\text{mHz} \rightarrow V3 = \begin{bmatrix} -0.1292 - 0.6080i \\ 0.4638 + 0.4138i \\ 0.4767 \end{bmatrix}$$

$$f = -1.953\ \text{mHz} \rightarrow V4 = \begin{bmatrix} 0.1292 + 0.6080i \\ 0.4638 - 0.4138i \\ 0.4767 \end{bmatrix}$$

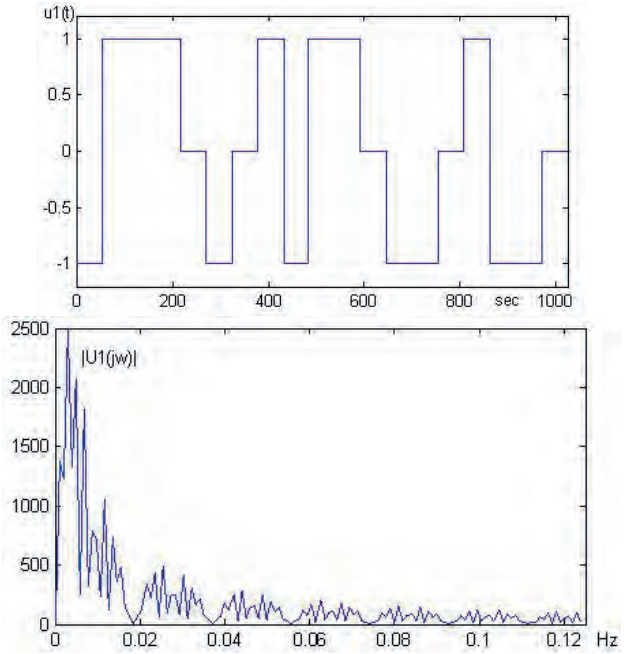

Figure 1. Plot of $u_1(t)$ and its FFT absolute values

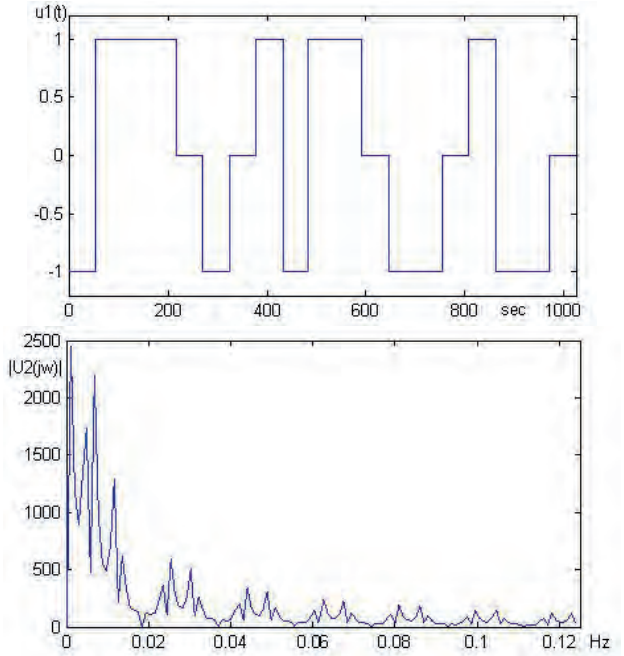

Figure 2. Plot of $u_2(t)$ and its FFT absolute values

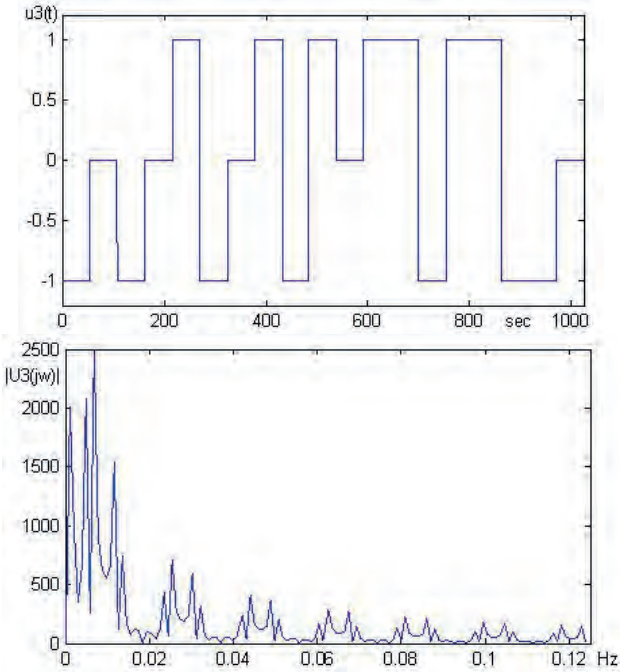

Figure 3. Plot of $u_3(t)$ and its FFT absolute values

$$f = 2.9295\,\text{mHz} \rightarrow V5 = \begin{bmatrix} 0.7959 - 0.4854\text{i} \\ 0.2356 + 0.2452\text{i} \\ 0.1240 \end{bmatrix}$$

$$f = -2.9295\ \text{mHz} \rightarrow V6 = \begin{bmatrix} 0.7959 + 0.4854\text{i} \\ 0.2356 - 0.2452\text{i} \\ 0.1240 \end{bmatrix}$$

$$f = 3.9062\,\text{mHz} \rightarrow V7 = \begin{bmatrix} 0.4708 + 0.4607\text{i} \\ 0.5799 - 0.3605\text{i} \\ 0.3159 \end{bmatrix}$$

$$f = -3.9062\,\text{mHz} \rightarrow V8 = \begin{bmatrix} 0.4708 - 0.4607\text{i} \\ 0.5799 + 0.3605\text{i} \\ 0.3159 \end{bmatrix}$$

$$f = 4.8825\,mHz \rightarrow V9 = \begin{bmatrix} 0.3349 - 0.5104i \\ 0.5011 - 0.1615i \\ 0.5917 \end{bmatrix}$$

Based on these 9 eigenvectors we assemble 9 vectors $W(\omega_k)$ that lead to the following **H** matrix, appendix equation (24)
that has rank 9. Hence, we conclude that **u**(t) is persistently exciting of order 3.
Moreover, if an iterative procedure of the proposed checking algorithm is executed for an order higher than 9 (increasing the value of *n* until a value is reached beyond which no further evidence of persistence is found) it is found that **u**(t) is persistently exciting of order 38.
Moreover, this example shows that the spectral analysis based on Fourier concept is able to deal with sharp changing pulses.

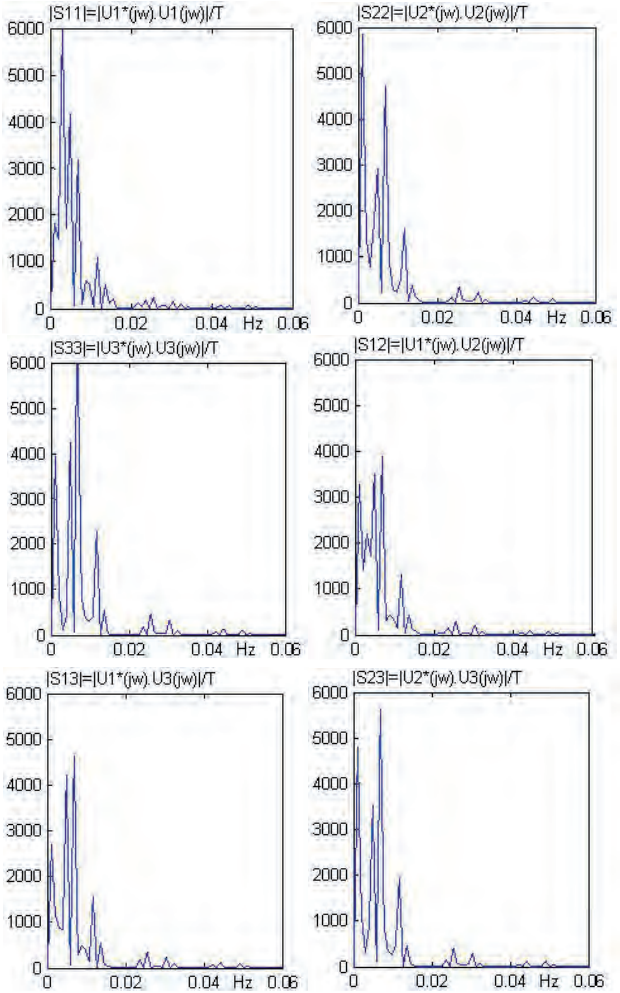

Figure 4. Plot of components of the spectral density matrix

6. Conclusion

It has been shown that the assumption used to check the persistency, found in literature, that the $\mathbf{\Phi_u}(\omega)$ has to be positive definite in *n* distinct frequencies does not apply for a sampled deterministic signal because its FFT-based estimate always has rank 1. Then, based on a sufficient condition, a strategy was developed to show that if a deterministic *m*-vector signal ***u*** has *mn* distinct frequencies which verify the condition of linear independence of $W(\omega_k)$ – defined in equation (14) - it is persistently exciting of order n, despite the fact that its $\mathbf{\Phi_u}(\omega)$ is not positive definite for these *mn* frequencies.

7. References

[1] K. S. Narendra & A. M. Annaswamy, Stable Adaptive Systems, Prentice-Hall, New Jersey, 1989.
[2] S. Sastry & M. Bodson, Adaptive Control – Stability, Convergence and Robustness, Prentice-Hall, New Jersey, 1989.
[3] P. A. Ioannou and J. Sun, Robust Adaptive Control, Prentice-Hall, New Jersey, 1996.
[4] T. Söderström & P. Stoica, System Identification, Prentice-Hall, London, 1989.

[5] L. Ljung, System Identification, 2nd Ed. Prentice-Hall, New Jersey, 1999.
[6] T. Söderström, U. Soverini and K. Mahata, Perspectives on Errors-in-variables Estimation for Dynamic Systems, Signal Processing, vol. 82: 1139-1154, 2002
[7] I. M. Y. Mareels & M. Gevers, Persistency of Excitation Criteria for Linear, Time-Varying Systems, Mathematics of Control, Signals and Systems, vol. 1: 203-226, 1988.
[8] J. S. Bendat & A. G. Piersol, Engineering Applications of Correlation and Spectral Analysis 2nd Ed., Wiley, New York, 1993.
[9] J. S. Bendat & A. G. Piersol, Random Data – Analysis and Measurement Procedures 3rd Ed., Wiley, New York, 2000.
[10] H. A. Barker, D. E. Rivera, A. H. Tan and K. R. Godfrey, Perturbation Signal Design, In proceedings of 14th IFAC Symposium on System Identification, Newcastle, Australia, 2006.
[11] D. C. Evans, D. Rees and D. L. Jones, Design of Test Signals for Identification of Linear Systems with Nonlinear Distortions, IEEE Trans. Instrumentation & Measurement, vol. 41 (6): 768-774, 1992
[12] R. Pintelon & J. Schoukens, System Identification: A Frequency Domain Approach, IEEE Press, New York, 2001.
[13] A. V. Oppenheim & A. S. Willsky, Signals & Systems 2nd Ed., Prentice-Hall, New Jersey, 1997.
[14] J. S. Walker, Fast Fourier Transforms, CRC Press, Boca Raton, Florida, 1991
[15] D. R. Brillinger, Time Series Data Analysis and Theory, Holt Rinehart Winston, New York, 1975.
[16] P. Naidu, Modern Spectrum Analysis of Time Series, CRC Press, Florida,1996.

Biography

Dr. W. C. Leite Filho received his Masters degree in 1982 and did his Ph.D from Federal University of Rio de Janeiro in 1991. He is currently working as Senior Researcher in the department of Space Systems of Aeronautics and Space Institute, São Paulo, Brazil. He has 100 publications in National and International journals and conferences to his credit. His areas of interest are in Guidance, Navigation, Control and Simulation of Aerospace Systems.

Appendix

$$\begin{bmatrix} \left(\sum_{i=1}^{m}\vartheta_i\sum_{k=1}^{n}m_{k_{1i}}(j\omega)^{-k}\right)^2 & \left(\sum_{i=1}^{m}\vartheta_i\sum_{k=1}^{n}m_{k_{1i}}(j\omega)^{-k}\right)\left(\sum_{i=1}^{m}\vartheta_i\sum_{k=1}^{n}m_{k_{2i}}(j\omega)^{-k}\right) & \cdots & \left(\sum_{i=1}^{m}\vartheta_i\sum_{k=1}^{n}m_{k_{1i}}(j\omega)^{-k}\right)\left(\sum_{i=1}^{m}\vartheta_i\sum_{k=1}^{n}m_{k_{mi}}(j\omega)^{-k}\right) \\ \left(\sum_{i=1}^{m}\vartheta_i\sum_{k=1}^{n}m_{k_{1i}}(j\omega)^{-k}\right)\left(\sum_{i=1}^{m}\vartheta_i\sum_{k=1}^{n}m_{k_{2i}}(j\omega)^{-k}\right) & \left(\sum_{i=1}^{m}\vartheta_i\sum_{k=1}^{n}m_{k_{2i}}(j\omega)^{-k}\right)^2 & & \vdots \\ \vdots & & \ddots & \vdots \\ \left(\sum_{i=1}^{m}\vartheta_i\sum_{k=1}^{n}m_{k_{1i}}(j\omega)^{-k}\right)\left(\sum_{i=1}^{m}\vartheta_i\sum_{k=1}^{n}m_{k_{mi}}(j\omega)^{-k}\right) & & \cdots & \left(\sum_{i=1}^{m}\vartheta_i\sum_{k=1}^{n}m_{k_{mi}}(j\omega)^{-k}\right)^2 \end{bmatrix} \equiv 0 \quad (19)$$

H =

$$\begin{bmatrix} -0.1976+0.0179i & 0.0089+0.0988i & 0.0494-0.0045i & -0.0771-0.3561i & -0.1781+0.0385i & 0.0193+0.0890i & 0-0.2790i & -0.1395 & 0+0.0698i \\ -0.1976-0.0179i & 0.0089-0.0988i & 0.0494+0.0045i & -0.0771+0.3561i & -0.1781-0.0385i & 0.0193-0.0890i & 0+0.2790i & -0.1395 & 0-0.0698i \\ -0.2027-0.0431i & -0.0144+0.0676i & 0.0225+0.0048i & 0.1379-0.1546i & -0.0515-0.0460i & -0.0153+0.0172i & 0-0.1589i & -0.0530 & 0+0.0177i \\ -0.2027+0.0431i & -0.0144-0.0676i & 0.0225-0.0048i & 0.1379+0.1546i & -0.0515+0.0460i & -0.0153-0.0172i & 0+0.1589i & -0.0530 & 0-0.0177i \\ -0.1213-0.1990i & -0.0497+0.0303i & 0.0076+0.0124i & 0.0613-0.0589i & -0.0147-0.0153i & -0.0038+0.0037i & 0-0.0310i & -0.0078 & 0+0.0019i \\ -0.1213+0.1990i & -0.0497-0.0303i & 0.0076-0.0124i & 0.0613+0.0589i & -0.0147+0.0153i & -0.0038-0.0037i & 0+0.0310i & -0.0078 & 0-0.0019i \\ 0.0921-0.0942i & -0.0188-0.0184i & -0.0037+0.0038i & -0.0721-0.1160i & -0.0232+0.0144i & 0.0029+0.0046i & 0-0.0632i & -0.0126 & 0+0.0025i \\ 0.0921+0.0942i & -0.0188+0.0184i & -0.0037-0.0038i & -0.0721+0.1160i & -0.0232-0.0144i & 0.0029-0.0046i & 0+0.0632i & -0.0126 & 0-0.0025i \\ -0.0851-0.0558i & -0.0093+0.0142i & 0.0024+0.0016i & -0.0269-0.0835i & -0.0139+0.0045i & 0.0007+0.0023i & 0-0.0986i & -0.0164 & 0+0.0027i \end{bmatrix} \quad (24)$$